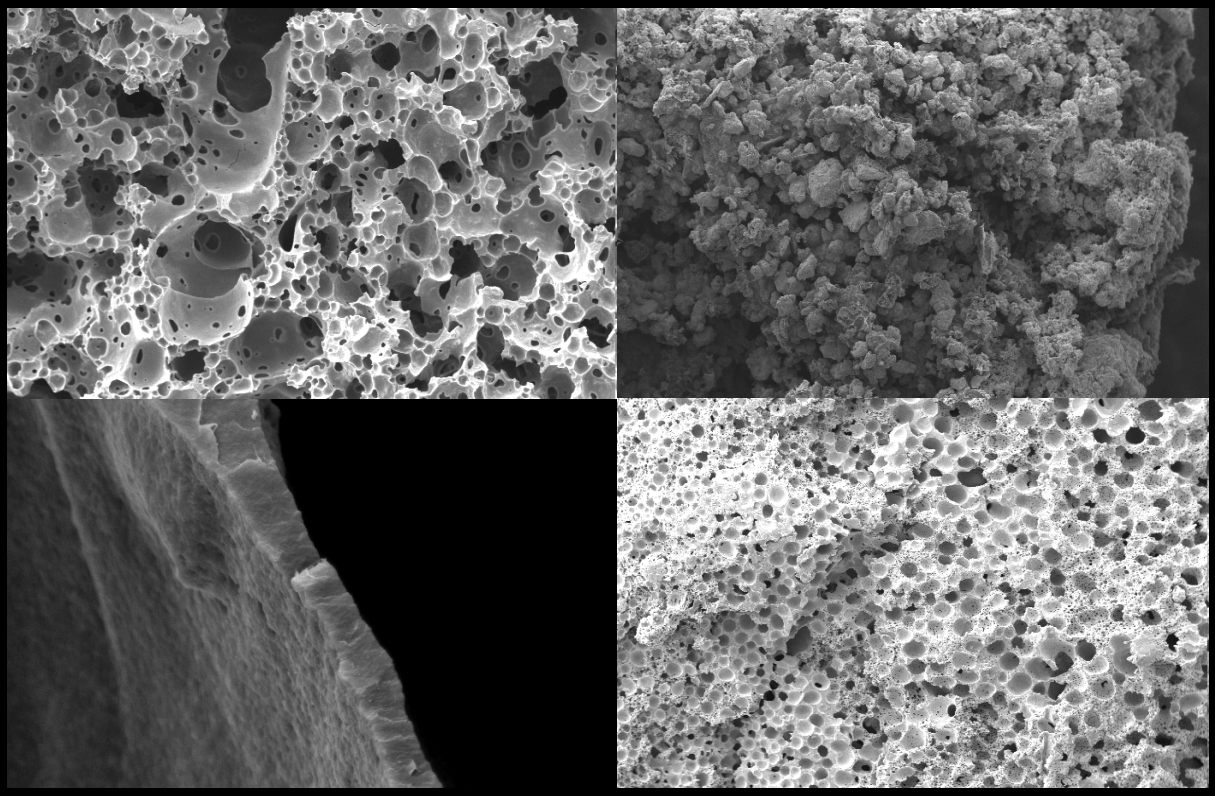

Maria Betânia Carreira de Matos

DRUG-ELUTING SILICA/POLY(α-ESTERS) BIOCOMPOSITE MATERIALS PREPARED BY GREEN TECNOLOGIES

SEPTEMBER 2012

· U C ·

UNIVERSIDADE DE COIMBRA

Biomedical Engineering Master Thesis

Drug-eluting silica/poly(α-esters) biocomposite materials prepared by green technologies

Supervisor: Hermínio José Cipriano de Sousa, PhD

Co-Supervisor: Mara Elga Medeiros Braga, PhD

Student: Maria Betânia Carreira de Matos

Abstract

The production of biodegradable composite-based scaffolds with application in tissue engineering may be accomplished by supercritical fluid (SCF) methods. Supercritical assisted- foaming occurs when the fluid phase is dissolved in the polymer phase melting it, and when the fluid is released, pores are formed within the material. Loaded inorganic particles may be prepared by SCF deposition, and finally, foaming impregnation and deposition can be used simultaneously to incorporate active substance in the composite. Processing with SCF has unique advantages over standard procedures, which include the absence of organic solvents, control over the morphology of internal porous architecture, and the ability to incorporate thermo- and chemical sensitive drugs. This work reports the development of dexamethasone-loaded composites prepared with poly(ε-caprolactone) (PCL) and mesoporous silica nanoparticles (SNPs), using SCF processes. Pure PCL and PCL/MCM-41 composite materials (90:10 and 70:30,wt.%) were processed by $scCO_2$ foaming at 35ºC, at different experimental pressure (14 and 25 MPa), processing time (2 and 14 hours) and depressurization (0.2 and 3.0 L/min) conditions. In addition, $scCO_2$ impregnation/deposition (SSI/SSD) method was used to load dexamethasone (DXMT) into MCM-41 and SBA-15 SNPs at 14 and 25 MPa for 14 hours and 0.2 L/min, and these were incorporated into PCL/DXMT physical mixture. All prepared materials were physically, thermally and chemically characterized. Drug release studies were performed in order to evaluate and to compare the obtained DXMT release profiles. Scaffolds morphology revealed small pores (46.5±6.6 Å) in samples with higher inorganic amount processed at higher pressure, longer exposition to $scCO_2$ and rapid depressurization rates. Other pores sizes up to 40 μm, and porosity between 12 and 55% were obtained, and pore volume increased from $9\pm2\times10^{-4}$ to 0.15±0.05 cm^3/g with increasing MCM-41 loading and pressure, as well as density that varied from 1.08 up to 1.30 g/cm^3. On the other hand, SEM pictures revealed pores smaller than 10 μm and larger than 400 μm, especially in 90:10,wt.% samples. Mechanical compression analysis showed that 90:10,wt.% samples are more resistant than the remainder, once the presence of a small amount of inorganic particles served as reinforcement matrix, displaying higher compressive modulus and compressive stress resistance, regardless the employed process conditions. Results demonstrated the viability of using $scCO_2$ impregnation/deposition and foaming methods for the development of DXMT-loaded PCL/SNPs biomaterials. DXMT scaffolds with different contents of previously loaded SNPs were produced and for the same period of time, 70:30,wt.% composites were able to release higher amounts of drug (14 μm/ml). Therefore, the materials used to produce composites (SNPs and PCL) allow obtaining distinguishable release and dissolution rates, and consequently different released amounts, which are potentially advantageous for use in pharmaceutical and biomedical applications.

Resumo

A produção de scaffolds compósitos biodegrádeveis com aplicação em engenharia de tecidos pode ser atingida por métodos de fluidos supercríticos (SCF). O supercritical assisted-foaming ocorre quando a fase do fluido se dissolve na fase polimérica fundindo-a, e quando o fluido é libertado, são formados poros no material. Partículas inorgânicas carregadas podem ser preparadas por deposição por SCF, e finalmente, foaming, impregnação e deposição podem ser usados simultaneamente para incorporar substâncias activas no compósito. O processamento com SCF tem vantagens únicas relativamente a processos convencionas, incluindo a ausência de solventes orgânicos, controlo da arquitectura interna dos poros, e a capacidade para incorporar fármacos sensíveis à temperatura e a químicos. Este trabalho descreve o desenvolvimento de compósitos carregados com dexametasona (DXMT) preparados com poly(ε-caprolactone) (PCL) e nanopartículas de sílica mesoporosa (SNPs), usando processos de SCF. PCL pura e materiais compósitos de PCL/MCM-41 (90:10 e 70:30,wt.%) foram processados por $scCO_2$ foaming a 35ºC, a diferentes pressões (14 e 25 MPa), tempo de processamento (2 e 14 horas) e taxas de despressurização (0.2 e 3.0 L/min). Adicionalmente, métodos de $scCO_2$ impregnação/deposição (SSI/SSD) foram usados para carregar DXMT nas SNPs de MCM-41 e SBA-15, a 14 e 25 MPa, 14 horas e 0.2L/min, e estas foram posteriormente incorporadas na mistura física de PCL/DXMT. Todos os materiais preparados foram caracterizados física, térmica e quimicamente. Estudos de libertação de fármaco foram efectuados de forma a avaliar e comparar os perfis de libertação de DXMT obtidos. A morfologia dos scaffolds revelou poros pequenos (46.5±6.6 Å) em amostras com maior quantidade de material inorgânico processadas a pressão elevada, exposição ao $scCO_2$ maior e taxas de despressurização rápida. Outros tamanhos de poros de até 40 μm, e porosidade entre 12 e 55% foram obtidos, e o volume de poros aumentou de $9\pm2\times10^{-4}$ para 0.15±0.05 cm^3/g com o aumento da quantidade de MCM-41 e da pressão, assim como a densidade que variou de 1.08 a 1.30 g/cm^3. Por outro lado, as fotografias de SEM revelaram poros menores que 10 μm e maiores que 400 μm, especialmente nas amostras 90:10,wt.%. A análise de compressão mecânica mostrou que as amostras 90:10,wt.% são mais resistentes que as restantes, uma vez que a presença de uma pequena quantidade de partículas inorgânicas serviu como matriz de reforço, exibindo maior módulo de compressão e maior tensão de compressão, independentemente das condições experimentais usadas. Os resultados demonstram a viabilidade da utilização dos métodos de $scCO_2$ impregnação/deposição e foaming para o desenvolvimento de biomateriais de PCL/SNPs carregados com DXMT. Foram produzidos scaffolds de DXMT com diferentes quantidades de SNPs carregadas previamente e, para o mesmo intervalo de tempo, os compósitos 70:30,wt.% foram capazes de libertar maiores quantidades de fármaco (14μg/ml). Desta forma, os materiais usados para produzir compósitos (SNPs e PCL) permitiram a obtenção de taxas de libertação e dissolução distintos, e consequentemente diferentes quantidades libertadas, que são potencialmente vantajosas para o uso em aplicações farmacêuticas e biomédicas.

Acknowledgements

In the end of this stage I must thank to everyone that contributed directly or indirectly to the accomplishment of this work.

To Prof. Hermínio Sousa for the enthusiasm, availability, guidelines and dedication. To Dr. Mara Braga for unconditional support, care (and reprimands), and for setting so much interest, and devotion in this work.

To my family: I owe them everything. Thank you for the persistence, opportunities, for making me grow up, for never giving up on me… A very special thanks to an extraordinary woman, her inspiring, encoring life, wisdom, and unreserved love - my grandmother.

To João Bessa, Rita Teixeira (and Miguel Alpendre), Carla "Tisha" Dinis (and Zé Nunes), Ana "Sissi" Silva, for all the love, critical-moments support, laughs, tears, and good moments over the years.

To the entire FeyeCon D&I family, without exceptions, for receiving so well, for making me feel at home, for the wonderful good mood, and for all the knowledge. A special thanks to Madalina, Iñaki (and the Two Top Managers (and one intern) super secret group), May Young, Andreas W., Frank vM, Lina, Rob, Wim, and Dennis S. I'm very grateful for the opportunity.

To my Amsterdam-ghetto-Gein housemates for the past 3 months: Sara Masiero, Michèle "ConstantFaith", Lisa Cosyn (and fatboy). It was a great pleasure to meet and to live with you. Thank you for all the *gezelleg* days! I couldn't make it without you!

To Laboratório de Alta Pressão e Tecnologia Supercrítica (LAPTS) group for the encouragement, knowledge sharing, and help throughout this process. To Dr. Ana Dias for all technic and theoretic help (and chocolates) and to Ana Cortez for all good and bad moments that made us both grow (and for testing my patience). To Eng. João Cortez for the availability and readiness to make the molds.

To Dr. Carmen Alvarez-Lorenzo, Pharmacy and Pharmaceutical Technology Department, University of Santiago de Compostela, and to Dr. Ana Paula Piedade, Mechanical Engineering Department, University of Coimbra, for the collaboration on this thesis.

Table of Contents

List of Figures

List of Tables

List of equations

List of Supplementary Data

Appendix A

Appendix B

Appendix C

Goals and Motivation

The purpose of this work was to develop a composite scaffold suitable for bone tissue engineering with the capability of release a certain drug with the appropriate kinetics. One of the main problems with current scaffolds is that they do not have high enough modulus for bone tissue applications and are fabricated by conventional techniques, which make use of high temperatures and organic solvents.

Furthermore, currently the implant/fixation device is either implanted for life and the bone would heal around it, or a second surgery is required to remove it once the surrounding bone is strong enough. Hence, this work arose from the need to develop new materials for application in regenerative medicine.

In order to overcome these drawbacks, scaffolds of polycaprolactone (PCL) combined with silica nanoparticles (SNPs) were created by supercritical CO_2 foaming, with an environmental acceptable method. PCL is known for its slow degradation rate and biocompatibility and SNPs are inorganic materials similar to that found in bone apatite and serve as reinforcement matrix; moreover, these SNPs have small pores, extensive surface area, making it suitable for drug delivery and augment bioavailability. Therefore, employing distinct supercritical conditions and amounts of SNPs, different release profiles would occur.

Supercritical fluids, more concretely supercritical carbon dioxide, are advantageous solvents to process polymeric and composite materials with adequate shapes and porosities, and to deposit/impregnate dexamethasone, at mild conditions.

Besides creating the aforementioned scaffolds, this work also consisted in chemical, physical and morphologic characterization these materials. Drug release assays were performed in order to study, not only the release kinetics but also supercritical deposition/impregnation efficiency.

1. Introduction

Tissue engineering is a promising approach that involves the use of scaffolds, biomaterials, cells and bioactive substances and that aims for repair, replace or regenerate damaged tissue or organs and involves the culture of living cells or a synthetic scaffold and subsequent implantation on the injured site (Jenkins, 2007). The rising importance of tissue engineering is due to the limited availability of organs for transplants and immune compatibility issues (Park *et al.,* 2007).

Tissue engineering constructs must be biocompatible and have the ability to mimic the natural body extracellular matrix, whose primary function is to act as a spatial template for cells that allow support, guidance and stability, aiming accurate regeneration and release precise amounts of bioactive substances, such as drugs and growth factors, at rates matching the physiological needs of the tissue. This supports the growing importance of controlled drug delivery in the field of tissue engineering (Vallet-Regí *et al.,* 2007, Tai *et al.,* 2007, Woods *et al.,* 2004, Roohani-Esfahani *et al.,* 2011, Collins *et al.,* 2008, Collins *et al.,* 2010, Vega-González *et al.,* 2008, Duarte *et al*., 2009).

As such, biomaterials have a direct impact on the quality of life of those people suffering from debilitating disease or reduction in bodily function (Long *et al.,* 2002). In the particular case of hard tissue applications, biomaterials should have low density, good mechanical resistance and biocompatibility (Liu *et al.,* 2004). Biomaterials are synthetic or natural materials intended to function appropriately in a bio-environment, and include any kind of material intended to restore/replace organ/tissue function. The most common examples include sutures, tooth fillings, needles, catheters, and bone plates (Park *et al.,* 2007). When engineering a device to restore the function of a body tissue, the major subjects concern mechanical properties, design, biocompatibility, biodegradability and pharmacological tolerance (eg. nontoxicity, noncarcinogenic and nonallergenic). Biocompatibility is a dynamic process that involves the time dependent effect of the host on the material and of the material on the host (Vallet-Regí *et al.,* 2007); it is understood as the inexistence of acute systemic toxicity, cytotoxicity, hemolysis, pyrogenicity, among others (Park *et al.,* 2007). The material should also have appropriate elasticity, yield stress, ductility, toughness, and wear resistance. It should also be amenable to be shaped at relative low cost and be readily available. The suitable design of an implant material should be aimed to provide the essential durability, functionality and biological response (Paital *et al.,* 2009).

To facilitate formation of new tissue in a scaffold, it should have highly interconnected pore network, exhibit adequate surface chemistry, and also provide mechanical integrity congruent with the defect site. Residence time in the injure site, which should match the time for the growth of new tissue, is determined by its degradation rate (Tai *et al.,* 2007, Woods *et al.,* 2004, Roohani-Esfahani *et al.,* 2011, Collins *et al.,* 2008, Collins *et al.,* 2010, Vega-González *et al.,* 2008, Meyer, 2009).

Pore morphology and porosity are important features that must be considered to the type of tissue being regenerated. While bone ingrowth prevails in structures with pore sizes of 450 μm, connective tissue grows preferentially in pores of 100 μm or less, and vascular infiltration ideally occurs within pores of 1000 μm. Fibro-cartilaginous tissue was also found to grow in structures with macropores (150–300 μm) highly interconnected by pores with less than 50 μm (Jenkins, 2007).

The proper function of the implanted material is, as well, dictated by its long-term biocompatibility (Vallet-Regí *et al.,* 2007, Vega-González *et al.,* 2008, Jenkis, 2007). Biological reaction begins with the rapid adsorption of certain proteins onto the surface of the material, followed by platelet adhesion. Immune and inflammatory cells act, isolating the foreign material in a fibrous capsule. This capsule is a barrier to drug delivery to the injured tissue and for nutrient to supply encapsulated cells; also, it can lead to formation of thrombi (Vallet-Regí *et al.,* 2007, Jenkins, 2007). Among the biomaterials that may display biocompatibility are silica-based systems (Vallet-Regí *et al.,* 2007).

The pore size also determines the size of the molecule that can be adsorbed into de matrix. Being a size-selective process, pores larger than the drug molecule are enough to allow the adsorption of the drug inside the pores (Vallet-Regí *et al.,* 2007). The actual trend in tissue engineering is based on the development of biodegradable scaffolds containing bioactive substances in order to control the biological activity of the injured site; thus, the compounds may be growth/differentiation factors or drugs (Meyer *et al.*, 2007; Duarte *et al.*, 2009), such as anti-inflammatory or corticosteroids.

1.1 Tissue Engineering: Hard-Tissues Application

Bone is a dynamic tissue that is constantly being formed and resorbed; this remodeling process is mainly governed by osteoblasts (derived from mesenchymal lineage cell) and osteoclasts (multinucleated giant cells) due to their resorptive-appositional activities, at a rate of approximately 2-10% per year. Skeletal tissues display different arrangement and porosity to maintain high vascularization and bone performance, including mechanical, biological and chemical functions, such as mechanical support, protection of organs and storage of mineral ions, namely calcium and phosphate (Izquierdo-Barba *et al.,* 2008, Jenkins, 2007].

Natural hard tissues in vertebrates are natural composite materials, composed of an organic matrix and an array of inorganic nanoapatites. The type I collagen molecules, the major component of the organic matrix, are bonded forming linear chains that are in turn arranged in fibers, giving rise to macroscopic structures and leaving small empty interstitial compartments. In this compartments are housed apatite particles; they are deposited during a controlled biomineralization process. The integration of both organic and inorganic phases at the nanometric scale modulates the mechanical properties of each type of bone (Izquierdo-Barba *et al*., 2008).

In this sense, composite materials contain two or more distinct constituent phases on a

scale larger than the atomic, and in which properties are significantly altered in comparison with those of a homogeneous material (Bronzino, 2003, Ratner, 2004). Composites consist of one or more discontinuous phases (usually harder and stronger, denominated as reinforcing material) surrounded by a continuous phase (termed matrix) (Ratner, 2004). Natural biological materials tend to be composites and include bone, wood, dentin, cartilage, and skin. The properties of these materials are highly anisotropic, and the only possibility to mimic them is to create composites (Ratner, 2004).

Organic-inorganic hybrid materials can be defined as materials with organic and inorganic components that are closely mixed. Hybrids are either homogeneous systems, derived from monomers and miscible organic and inorganic components, or heterogeneous systems (nanocomposites), where at least one of the domains has a dimension up to a few tens of nanometers. The properties of hybrid materials are not only the sum of the individual contributions of both phases, but synergy is elapsed from the coexistence of the two phases through size domain effects and nature of the interfaces (Vallet-Regí *et al.,* 2011). In particular, the properties of a composite material depend upon the shape of the heterogeneities, upon the volume fraction occupied by them, and upon the interface among the constituents (Bronzino, 2003, Ratner, 2004).

One of the constituents of composites may be polymers and they may be used to replace diseased organ function when they have biocompatible and biodegradable matrix, controllable degradation kinetics, 3D porous architecture to support cell attachment and proliferation. Surface chemistry should be appropriate for cell attachment, proliferation and differentiation. The choice of polymer is therefore of extreme importance in determining the success of the scaffold (Jenkins, 2007).

Linear aliphatic polyesters are straight-chain polymers in which monomers are joined by the ester bond. Commonly used linear aliphatic polyesters include polyglycolide or poly(glycolic acid) (PGA), poly(lactic acid) (PLA), polycaprolactone, poly(β-hydroxybutyrate), and poly(glycolide–trimethylene carbonate) (Lui, 2007).

Poli(ε-caprolactone), in particular, degrades significantly slower than PLA or PGA and *in vivo* tests have shown that it takes about 2–4 years to completely degrade. PCL materials and composites with other materials, such as hydroxyapatite, poly-l-lactides, and silica, have been used in a number of biomedical applications, such as scaffolding and repairing soft and bone tissues (Lui, 2007). PCL is currently used as a biodegradable tissue scaffold and likely to suffer catalyzed hydrolysis. Due to PCL hydrophobic and semi-crystalline nature, its degradation rate it's considerably slow, and therefore it is especially attractive for long-term applications. There are two distinct steps involved in poly-α-ester degradation: random hydrolytic cleavage and enzymatic fragmentation. The first one is initiated at the amorphous regions and it's auto-accelerated by carbonyl ends of polymeric chains. Bulk fragmentation origins fragments, whose size is dependent on the initial molecular weight, which are taken up by macrophages and degraded intracellularly. Mass loss begins when these

fragments' size is small enough to diffuse through matrix. Mass loss is only initiated 4-6 months later once fragments' minimal molecular weight should be around 5 kDa. The second step is characterized by cracks on the surface (Dash *et al.,* 2011). While the second step of degradation eliminates the need to remove the device, the permeability to low molecular weight drugs combined with the first step degradation step make PCL-based drug delivery systems (DDS) suitable for long period applications (Pitt *et al.*, 1990).

PCL exhibits low melting temperature of approximately 57 ºC as well as low glass transition temperature (T_g) of −60ºC; it has a high thermal stability (T_d ~350 ºC) compared with other polyesters (T_d ~ 235–255 ºC), which enables it to be processed using a variety of routes (Jenkins, 2007). Mechanically, PCL materials can be stretched approximately 30% elongation at a yielding stress about 11 MPa; the elastic modulus is about 0.3 GPa (Lui, 2007).

Currently, PCL is classified as non-toxic and tissue compatible by FDA but is not yet used extensively as a biomaterial. However, its high tendency to form compatible blends with a variety of polymers and may enhance its future biomaterial role (Jenkins, 2007).

SNP (Silica Nanoparticles) materials with 2D hexagonal structures, such as MCM-41 and SBA-15 silicas, have attracted interest in the biomedical field. Mesoporous materials exhibit order at mesoscopic scale and disorder at the atomic scale. The synthesis of this type of materials is based on the use of surfactants for the assembly and condensation of the inorganic precursor. Surfactant removal leaves a network of cavities within the silica framework, which determines the final physical and chemical properties (Vallet-Regí *et al.,* 2011). Mesopores diameters can be tuned from 1.5 nm to several dozens of nanometers, by altering processing parameters: chain length of the surfactant, employ polymeric structure-directing agents or solubilize auxiliary substances. The stability of the pore structure varies with thermal treatment, which determines the thickness of the pores wall and, consequently, the potential kinetic release of a drug (Vallet-Regí *et al.*, 2007).

Their large surface areas and pore volumes, allow adsorption of a wide range of molecules/drugs (Lin *et al*., 2010, Zhao *et al.*, 2011). SNPs have the ability of hosting different guest molecules and their adequate bioceramic characteristic may allow their use in the repair of bone defects. They may control bioavailability of the drug and fill the gap where some conventional polymers fail (Vallet-Regí *et al.,* 2007). Therefore, these materials have the potential to become vehicles for biomedical imaging, real-time diagnosis, and controlled delivery of multiple therapeutic agents, (Zhao *et al.*, 2011).

Drug-loading process is mainly governed by the adsorptive properties of mesoporous materials, where the surface becomes the most determining factor for the amount of adsorbed drug (Vallet-Regí *et al.,* 2007). Host-guest interaction must also be taken into account in drug delivery/loading: it takes place between the silanol groups on the surface and the functional groups of the drug. The parameters that govern drug

adsorption and release process mainly depend on the host-matrix (Vallet-Regí *et al.,* 2011). The drug release from different mesoporous silica matrices has been found to be controlled not only by host-guest interaction but also by diffusion, by pore architecture, as well as to depend on properties of the dissolution medium (Heikkila *et al.*, 2007).

Despite these advantages, the influence of physicochemical factors (as geometry, pore size, porosity and surface functional groups) still needs to be further assessed. Yu *et al.* (2011), investigated the porosity, shape, and surface modification effects on cellular toxicity/ hemolytic activity on macrophages, cancer epithelial cells, and human erythrocytes. The toxicity was found to be cell-type dependent, which can be due to the difference in the physiological function of each cell type (Yu *et al.*, 2011). On the other hand, Zhao *et al*. (2011) initial studies with red blood cells suggested that MCM-41 and SBA-15 nanoparticles were safe (not hemolytic) in contrast to amorphous silica. They latter reported that hemocompatibility of MSNs (mesoporous silica nanoparticles) also depends on the size of the nanoparticles, but the lack of hemolysis did not warrant the lack of interactions between the particles and the red blood cells (RBCs), which may be the cause of hemolysis in intravenous applications. In this sense, the same research group compared the size- and surface-dependent hemocompatibility of MCM-41 and SBA-15 and showed that MSNs are surrounded by RBCs, and concluded that this process is governed by two opposing forces: the attractive interaction between MSNs-RBCs and the bending of the cell membrane. They established that only small MCM-41 might be considered as potentially safe candidates for intravascular drug delivery. The effect of surface functional groups was also investigated. The blockage of the surface silanols with organic groups reduces their interactions with RBC membranes (Zhao *et al.*, 2011). Other authors also reported this effect (Lin *et al.*, 2010).

Bioactive molecules can be incorporated into scaffoldsand scaffolds can be prepared from a wide diversity of materials: metals, ceramics, polymers, and composites (Duarte *et al.*, 2009). Small molecular weight dexamethasone (DXMT) is widely used in hard tissue applications. This glucocorticoid is used in osteogenic media to improve stem cell differentiation towards the osteogenic lineage (Duarte *et al.*, 2009, Takahashi *et al.*, 2010). It is also used in many other medical conditions, such as arthritis rheumatoid, (Provan *et al.,* 2010) as well as to minimize myocardium acute inflammatory response in cardiac pacing patients (van de Beek *et al.,* 2007). It is also used in people undergoing chemotherapy to counteract side effects (Harousseau *et al.,* 2006). Before and/or after dental surgery (Schmelzeisen *et al.,* 2004) patients are often medicated with this drug. In addition, rare disorders of glucocorticoid resistance (Chrousos *et al.,* 1993), and premature birth risk to mature fetus lungs (Bloom *et al.,* 2001) are treated with DXMT.

1.2. Fabrication of Hard Tissue Engineering Scaffolds

As previously referred, high porosity and pore interconnectivity, as well as 3D porous structure, are extremely important for tissue regrowth. Thermally induced phase separation, compression and injection moulding, extrusion, electrosppining, foaming, solvent casting-particle leaching among others, allow the conventional production of these 3D structures. The main inconvenient rely on the usage of organic chemicals/solvents and/or elevated temperatures (Duarte *et al.*, 2009, Tai *et al.*, 2007, Jenkins *et al.*, 2006). When sensible molecules, such as drug or growth factors, are intended to be incorporated in a certain material, these disadvantages are more clear, because they can easily degrade by heat or chemicals (Woods *et al.* 2004, Duarte *et al.,* 2009). Also, when large amounts of organic solvents are used, additional steps of extraction/purification may be required (Woods *et al.*, 2004).

1.2.1. Alternative Supercritical Fluids Processing

SCFs are unique solvents with tunable properties widely explored in various applications. In particular, supercritical carbon dioxide is inexpensive, non-toxic, non-flammable and readily available in high purity and is a ‘‘generally recognized as safe” (GRAS) solvent (Yañez F. *et al.*, 2011). Moreover, $scCO_2$ combines gas-like transpot properties, and liquid-like density above its critical pressure (7.4 MPa) and temperature (31.1ºC) conditions (Tai *et al.,* 2007, Woods *et al.,* 2004, Shieh *et al.,* 2009, Jenkins *et al.,* 2006, Xu *et al.,* 2004, Morèrea *et al.,* 2011). It has been explored as a solvent, anti-solvent or plasticizer for polymer processing, polymerization, modification and extraction due to its advantages over common solvents (Tai *et al.,* 2007, Kiran 2009).

The use of SCFs is particularly important when the viscosity of the bulk polymer is relatively high, as in the case of high molecular weight polymers. SCF can facilitate processing by acting as a solute, reducing the intermolecular interactions and increasing the chain separation, acting as a molecular lubricant (Jenkins *et al.,* 2006, Jenkins, 2007). This technology provides a clean way to process thermally labile/unstable biological compounds, to produce particles for controlled delivery in the body (Tai *et al.,* 2007, Woods *et al.,* 2004, Braga *et al.,* 2008).

Most pharmaceutical compounds and polymers present low solubility in $scCO_2$, though the solubility of $scCO_2$ in many polymers usually may be substantial; pressure becomes an additional key parameter that changes solvent properties. Without changing the type of fluid, the solvent properties can be tuned by varying its density, contrarily to traditional methods and solvents (Kiran, 2009, Braga *et al.,* 2008).

In the beginning of the process, solubilized $scCO_2$ can plasticize amorphous and semi-crystalline polymers, leading to a decrease in T_g, and can also reduce polymer melt viscosity, effectively melting them (Tai *et al.,* 2007, Woods *et al.,* 2004, Léonard *et al.,* 2008, Collins *et al.,* 2008, Kiran, 2009). Furthermore, crystallization temperature (T_c) is lowered from its initial value (Kiran, 2009), and it is also assumed that the melting temperature (T_m) of semi-crystalline polymers is lowered. $ScCO_2$ penetrates preferentially the amorphous phase of semi-crystalline polymers because of the

increased gas dissolution in those regions. Plasticization of the amorphous region increases the mobility of the polymer chains and enables them to rearrange into a more ordered configuration in the end, which in turn may induce crystallization and associated changes in morphology (Jenkins, 2007).

Thus, at the end of the process, upon depressurization, the polymer phase is supersaturated with CO_2, resulting in thermodynamic instability. The consequent pressure-induced phase separation increases the T_g. As the gas leaves the polymer phase and nucleation of gas bubbles occurs, leading to the formation of foams; by varying depressurization rate (Woods *et al.,* 2004) and amount of gas incorporated (Collins *et al.,* 2008) pore size can be controlled.

The number and size of formed pores is defined by the competition between growth rate and bubble nucleation rate. The homogeneous nucleation theory partially explains pores formation: the energy barrier for nucleation is a function of the extent of supersaturation; it is also directly related with the interfacial tension between the newly formed gas bubble and its surrounding material. Therefore, lowering interfacial tension results in the decrease of the nucleation energy barrier and the consequence is the formation of more stable gas nuclei. As more bubbles start to nucleate, the amount of gas available for growth is divided into more cells and, thus, foams with smaller pore diameters are obtained. Thus, when the pressure-drop increases (higher depressurization rates) the energy barrier for nucleation decreases, leading to an increase of the nucleation rate and to smaller bubbles (Léonard *et al.,* 2008, Tsimpliaraki *et al.,* 2011, Jenkins *et al.,* 2006).

This nucleation stage involves clustering of CO_2 molecules, which may occur homogenously and/or heterogeneously (Jenkins 2006). Studies indicate that the introduction of the dispersed inorganic material into the polymer matrix favors heterogeneous nucleation, by acting like an impurity. Hence, concurrent homogeneous and heterogeneous nucleation mechanisms occur upon phase separation of the polymer–CO_2 solution. Homogeneous nucleation occurs once the bubble radius exceeds a critical value when stable CO_2 nuclei form in the bulk plasticized polymer; heterogeneous nucleation, on the other hand, occurs when CO_2 bubbles nucleate on the surface of the dispersed nanoparticles or in preexisting microvoids close to the nanoparticles. Both mechanisms compete for available CO_2 molecules during depressurization but heterogeneous nucleation is energetically favored over homogeneous nucleation, since it typically requires a lower activation energy barrier (Léonard *et al.,* 2008, Tsimpliaraki *et al.,* 2011, Jenkins *et al.,* 2006).

As such, SCFs technology may provide the ability to control polymeric foam characteristics, such as pore size and degree of crystallinity, to produce a scaffold with the appropriate properties for tissue regeneration (Jenkins, 2007) and the ability to impregnate sensible substances into the melted polymer (Woods *et al.,* 2004, Léonard *et al.,* 2008, Xu *et al.,* 2004, Collins *et al.,* 2008, Braga *et al.*, 2008).

Conventional impregnation/deposition consists on the immersion a polymeric or inorganic matrix in a solution, which can be organic or aqueous containing a

dissolved substance. The conventional method makes sometimes use of toxic organic solvents (specially for poorly water soluble drugs), which have to be removed by an additional extraction step that can degrade substances, or induce drug thermal/chemical degradation, undesired substance reactions, substance/solvent dissolution, or heterogeneous substance dispersion (Duarte *et al.,* 2009, Natu *et al.,* 2008).

The use of compressed fluids (like carbon dioxide) as mobile phase, at temperatures and pressures near or above their critical values, can facilitate the diffusion of the substance and improve impregnation/deposition rate. Swelling the polymer matrix also facilitates the diffusion of the substance and improves impregnation rate. In the case of inorganic matrixes, there is no morphological alteration of the host matrix and the substance tends to be deposited on the surface (Duarte *et al.,* 2009, Natu *et al.,* 2008, López-Periago *et al.*, 2009, Yañez *et al.*, 2011, Belhadj-Ahmed *et al.* 2009, Smirnova *et al.* 2004).

Supercritical solvent impregnation/deposition (SSI/SSD) has already proved its feasibility and advantages for the development of drug delivery systems without significantly alter and or damage the constituents of the system. Also, drug loading, depth of penetration and homogeneity of drug dispersion can be controlled in relative short times, without solvent residues, by controlling operational conditions. SSI/SSD also allows previous preparation of the polymeric, inorganic or composites matrix and subsequently impregnate it with the intended drug (Braga *et al.*, 2008, Natu *et al.,* 2008, Yañez *et al.*, 2011).

SCF, especially $scCO_2$, have been identified as prime candidates to develop alternative clean processes for the preparation of drug-loaded polymeric matrices (Duarte *et al.,* 2009). However, even though CO_2 is the mostly used compressed fluid, the main drawbacks concern its difficulty to dissolve into high-molecular weight compounds and its non-polarity and absence of specific solvent-solute interaction that would lead to high impregnation/deposition yields. One strategy is to add small amounts of co-solvents to increase the substance solubility in $scCO_2$ and improving the $scCO_2$ solvent power (Natu *et al.,* 2008). Thus, SSI/SSD is feasible when the pharmaceutical compound is soluble in CO_2 (Duarte *et al.,* 2009).

Even though SCFs improve impregnation of some hydrophobic drugs, they may not considerably increase the compatibility of the host to the additive. SSI/SSD is an adaptable method to impregnate/deposit substances by varying depressurization rate, time of process, or by changing pressure and temperature, leading to density alterations and, therefore, drug solubility in the SCF (Kiran 2009, Braga *et al.*, 2008).

2. Materials and Methods

2.1. Chemicals

The PCL pellets (M_w of 45000 and 14000 Da), dexamethasone (purity ≥98%), methanol, acetone and mesoporous silica nanoparticles MCM-41 (pore volume 0.98 cm^3/g and 2.3-2.7 nm of pore size, surface area of 1000 m^2/g) were supplied by Sigma-Aldrich. SBA-15 SNPs were provided by ClaytecInc (average BJH Framework Pore Size 8.5 nm, total pore volume 0.93 cm^3/g, surface area 718 m^2/g). Panreac supplied ethanol (99.5% purity). CO_2 was obtained from Praxair with purity of 99.998%. Dialysis membranes (molecular weight cut-off of 8000 Da) and clamps were supplied by Spectrum Laboratories.

2.2. Methods

2.2.1. Polymer Preparation

Preliminary SCF assays were preformed with PCL in pellet form and in powder form, and in order to facilitate the physical mixture of PCL and SNPs during the $scCO_2$ processing, PCL was powderized. Thus, dissolution of 12.5 g of PCL in ~200 ml acetone followed by precipitation with ~ 10 ml of methanol and the same volume of water was preformed. For the low-molecular weight PCL, no anti-solvent was necessary: it dissolved and precipitated in the presence of acetone. After precipitation, samples were centrifuged at 5000 rpm for 10 min and the supernatant was removed. PCL powder was allowed to dry at room temperature and pressure in petri dishes for approximately one week, then stored in glass vials.

2.2.2. Supercritical Fluid Processing

Generally and as represented on Figure 1, supercritical foaming and impregnation/deposition were performed using a discontinuous supercritical solvent impregnation unit. The intended material (~1.5g) was loaded into a temperature controlled high-pressure cell (23 cm^3). Afterwards, CO_2 was introduced in the high-pressure cell at the desired pressure and temperature. Magnetic stirring (900 rpm) was used to solubilize the drug and, in its absence, to homogenize the high-pressure mixture. After the processing time, the compressed fluid was removed at the pre-established rate. Processed material was recovered and stored in glass vials.

$scCO_2$-assisted Foaming - Experimental conditions were varied according to the information provided by literature (Shieh *et al.*, 2009, Léonard *et al.*, 2008, Xu *et al.*, 2004, Duarte *et al.*, 2009) and $scCO_2$ properties in order to optimize SCF foaming. Only 45000Da PCL was used because the low molecular weight polymer after processed with MCM-41 appeared to disrupt. Thus, for the same temperature (35ºC), two pressures and two different proportions of PCL:MCM-41 were studied: 14.0 MPa and 25.0 MPa (0.801 and 0.901 g/cm^3, correspondingly), 70:30,wt.% and 90:10,wt.%, respectively; PCL and MCM-41 SNPs were physically mixed in a glass vial prior to $scCO_2$-assisted foaming and then introduced in high pressure cell. Also, for each

parameter previously mentioned, the process time and depressurization rate were varied: 2 and 14 h and 0.2 and 3.0 L/min, respectively. Moreover, control samples were processed for the same conditions where PCL:MCM-41 ratio was 100:0. All the assays were performed in duplicate.

$scCO_2$ Impregnation/Deposition - DXMT was loaded into pure mesoporous MCM-41 and SBA-15 SNPs by $scCO_2$ impregnation/deposition, at the previously mentioned pressures and temperature, for 14 h with depressurization rate of 0.2 L/min. SNPs (~15 mg) were placed into sealed dialysis membranes and then introduced in a high pressure view-cell which was previously loaded with ~9 mg of DXMT. DXMT-loaded SNPs were then incorporated into DXMT/PCL physical mixtures using $scCO_2$-assisted foaming and again at the same processing conditions. Physical mixtures PCL/DXMT were also foamed.

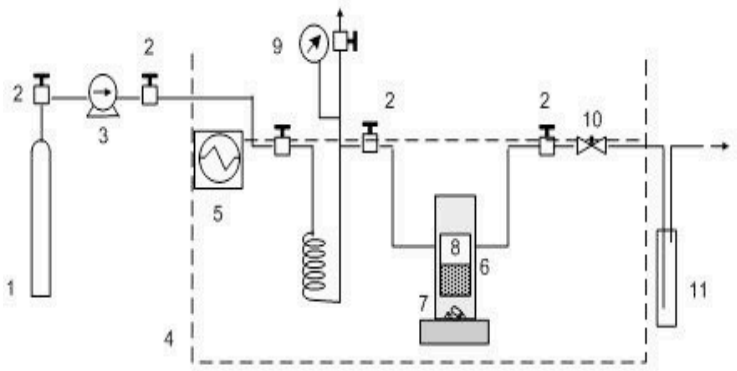

1- CO_2 reservoir
2- Valves
3- High-pressure CO_2 pump
4- Water bath
5- Temperature controller
6- High-pressure stainless steel cell
7- Magnetic stirrer
8- Sample
9- Pressure transducer
10- Needle valve
11- Glass trap

Figure 1 - Schematic diagram of the experimental supercritical foaming and impregnation/deposition unit.

Therefore, the production of drug loaded polymeric and composite materials with distinct release behaviors by $scCO_2$ foaming/SSI/SSD process was the main goal of this work (Figure 2). Several experimental conditions were applied, and characterization methods were performed in order to investigate the most suitable for hard-tissues applications.

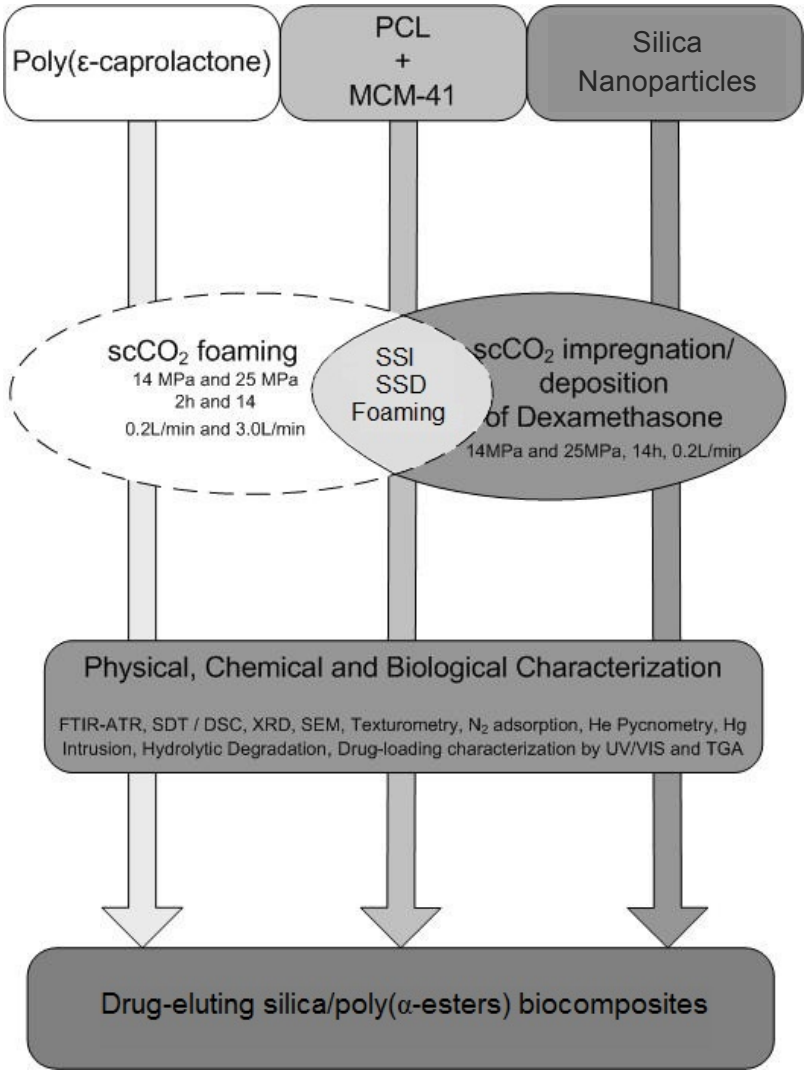

Figure 2 – Diagram of the process used to prepare composites by green technologies.

2.3. Characterization

FTIR-ATR spectroscopy measurements were performed on a Jasco FTIR spectrometer (Infrared Spectrum, Jasco, 4200 type A) using the Attenuated Total Reflectance (ATR) technique. The spectra were obtained at a 4 cm^{-1} resolution, 256 scans and processed by Jasco Spectra Analysis.

Thermal behavior of PCL-pellet, PCL-powder and $scCO_2$ processed material was determined on a Simultaneous Differential Thermal equipment (TA Q600) using standard alumina pans. Measurements were made on 7-11 mg of samples in the temperature range between 25 and 700 ºC at a heating rate of 2 ºC/ min. The instrument was calibrated with indium. Mass loss, characteristic temperatures and enthalpies were calculated using the software TA Universal Analysis. The results are the average and standard deviation of two samples.

PCL and composites crystalline phases were compared before and after foaming experiments using a Philips X'Pert diffractometer with Co radiation ($\lambda_{K\alpha 1}$ = 0,178896

nm and $\lambda_{K\alpha 2}$ = 0,179285 nm). 2θ values were varied from 6º up to 60º. Acquisition step was 0.004º and acquisition time was 1s/step (40kV and 35mA).

Average pore diameter, pore volume and surface area were determined by nitrogen adsorption using a ASAP 2000 Micromeritics, model 20Q-34001-01. Surface area was determined by the Brunauer, Emmet and Teller (BET) method, pore volume by the Barret, Joyner and Halenda (BJH) method, and average pore diameter was calculated by BET. Pore size distribution, total pore volume and porosity were determined by mercury intrusion. Apparent and bulk densities were also determined by this method using Autopore IV 9500 Micromeritics. The density of the foams was measured by helium picnometry (Quanta-Chrome, MPY-2). For these experiments samples were cut into small pieces of approximately 0.5 mm of diameter and 1 cm of height. The results are the average and standard deviation of two samples.

Compression properties were examined employing a TA.XT plus texture analyzer (Texture Technologies). Samples were analyzed inside glass vials to avoid sample movements. The analytical probe (P/10, 1 cm diameter) compressed each sample at a rate of 1 mm/s and a depth of 3 mm, with 5 gf of activation force. Compressive stress and modulus were determined according to other works previously reported (Baker *et al.*, 2009, Mathieu *et al.*, 2005, Georgiou *et al.*, 2006). The compressive modulus was calculated (until 10 % of strain) as the slope of the linear region of the stress vs. strain plot, and the presented data are the average and standard deviation of two samples.

Materials morphologies were evaluated examining the fracture surfaces by scanning electron microscopy (SEM). Samples were freeze-fractured in liquid nitrogen and the obtained cross-sections were examined by SEM (Philips XL30, 10kV), after gold-sputtering for 25s (gold thin film of 10-20 nm thick). SNPs presence was confirmed by image analysis of backscattered electrons and by EDX.

Drug sorption studies were preformed in order to determine the drug loading ability of MCM-41 and SBA-15 in conventional liquid solvents. Thus, ~100 mg of MCM-41 and SBA-15 was immersed into different dexamethasone solutions: aqueous and ethanolic solutions (26 μg/ml). At predetermined time intervals, an aliquot of the liquid media was read in a UV-Vis spectrophotometer (Jasco, Model V650, Japan) at fixed wavelength (242 nm). After 72 h the samples were centrifuged, the supernadant was removed and the material was allowed to dry in a oven at 37 ºC. The results are the average and standard deviation of three samples.

Drug release assays from loaded SNPs were preformed by placing ~15mg of sample inside dialysis membranes. Again, at predetermined time intervals, an aliquot of the liquid media was read in the UV-VIS spectrophotometer. Every 24h the release media was replaced by fresh Milli-Q water, and after 72h, samples were leached out until no drug could be detected. The analysis was preformed in quadruplicate and results are the average and standard deviation of at least two samples. In the case of PCL and composites, ~15 mg with approximately 2 mm of thickness were introduced inside dialysis membrane. Aliquots of the release media were read in the UV-VIS

spectrophotometer during one week. The analysis was preformed in triplicate and results are the average and standard deviation of at least two samples

The sorption and release of dexamethasone was described using a zero-order kinetics equation 1 where M_t and M_∞ represent the cumulative (absolute) amount of drug released at time *t* and at infinite time, respectively, *k* is a kinetic constant that incorporates the structural and geometric characteristics of the delivery device (that includes polymer and drug), and *n* is the release exponent, which can provide information about the drug release or sorption mechanism from liquid solutions. Some release processes are included between the Fickian diffusion and the zero-order kinetics. The power law translates this behavior, and this relationship is only valid, in most cases, for the first 60% of the drug released. (Braga *et al.*, 2008, Dias *et al.*, 2011, Natu *et al.*, 2008, Yañez *et al.*, 2011):

$$\frac{M_t}{M_\infty} = kt^n \qquad \textbf{Equation 1}$$

Other equations were also used to determine diffusion coefficients (*D*) from the resulting slopes of the polymeric and composite systems:

$$\frac{M_t}{M_\infty} = 4\left(\frac{Dt}{\pi l^2}\right)^{1/2} \qquad \textbf{Equation 2}$$

$$\frac{M_t}{M_\infty} = 1 - \left(\frac{8}{\pi^2}\right)e^{-\frac{Dt\pi^2}{l^2}} \qquad \textbf{Equation 3}$$

where *l* is the thickness of the sample (~2 mm). Equation 2 is usually valid for the first 60 % of the total release ($M_t/M_\infty \leq 0.6$) while Equation 3 can be applied for the last 40 % of the total release ($M_t/M_\infty \geq 0.4$) (Yañez *et al.*, 2011, Dias *et al.*, 2011, Siepmann *et al.,* 2011). In order to use these equations, slab geometry was considered. Diffusion coefficients were calculated from the average of the obtained values.

Calibration curves were determined in order to calculate the drug amount in sorption and release experiments (Appendix A1 and A2).

3. Results and Discussion

3.1. Fourier Transform InfraRed – Attenuated Total Reflectance

Chemical composition analysis was preformed by FTIR in order to investigate if there was any chemical change during the $scCO_2$ process, and the spectra are presented in Figure 3.

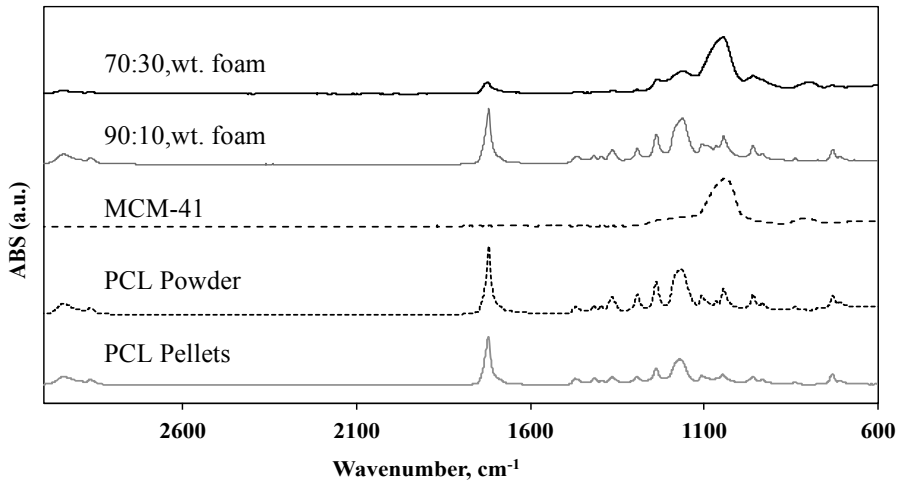

Figure 3 - FTIR-ATR spectra of the prepared composite material

The characteristic pure PCL crystalline phase peaks are represented by the carbonyl group stretching at 1727 cm^{-1} and by the C–O and C–C stretching vibrations at 1293 cm^{-1}. Other representative peaks are present at 1240 and 1170 cm^{-1} (corresponding to the asymmetric and symmetric COC stretching) at 1190 cm^{-1} (OC–O stretching) and at 1157 cm^{-1} (C–O and C–C stretching in the amorphous phase) (Elzubair *et al.*, 2006). Pure MCM-41 bands are represented by Si–O asymmetric stretching (at 1090, 1223 cm^{-1}), Si–O symmetric stretching (at 800 cm^{-1}) (Anunziata *et al.*, 2009). In PCL/MCM-41 composites (30 wt.%) it is clear the presence of both materials due to the evident superposition of their individual characteristic bands. However and in the case of 90:10,wt.% the characteristic bands of silica cannot be distinguished which is probably due to fact that SNPs are well dispersed in the polymeric matrix. Nevertheless, the presence of SNPs was confirmed by SEM-EDX (Figure 4) and by SEM-BSE image analysis. Finally and as expected, no apparent chemical modifications were observed in PCL.

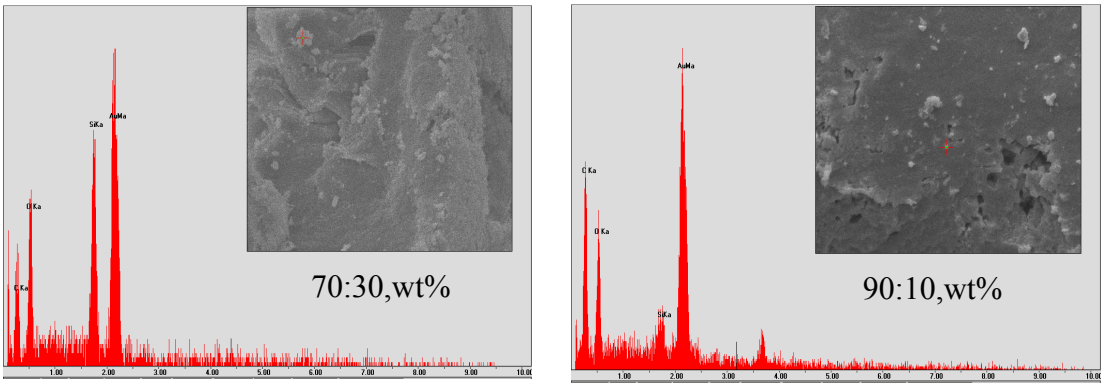

Figure 4 - SEM-EDX of composite samples used to confirm the presence of SNPs.

3.2. Thermal Characterization and Crystallinity

TGA analysis shows that the samples mass loss correspond to the employed PCL:MCM-41 ratio. Samples with 70wt.% of PCL show a corresponding mass loss was of 71.2% of the total mass. When concerning 90:10,wt.% samples, the residual mass corresponded to 9.8% and processed PCL, PCL-powder and PCL-pellet showed mass losses of 99.7%.

Table 1 – Thermogravimetric analysis results: mass loss

Sample	Mass loss, %
70:30,wt.	71.2 ± 3.5
90:10,wt.	90.2 ± 3.4
PCL	99.7 ± 0.6

Double melting peaks (exemplified in Figure 5) occurred in all samples containing PCL, before and after CO_2 treatment, indicating that the sample underwent through crystallization. According to Kiran *et al.* (2008), multiple melting peaks are characteristic in crystals formed under pressure in melting or formed from solutions at high pressure, and points out three explanations: either occurs re-crystallization of metastable crystals upon eating (throughout which the fold length of the crystals increases and the melting temperature shifts to higher values); crystallization in amorphous regions; or crystals with different lamellar thickness are produced and may appear from different crystallization kinetics and /or depressurization paths.

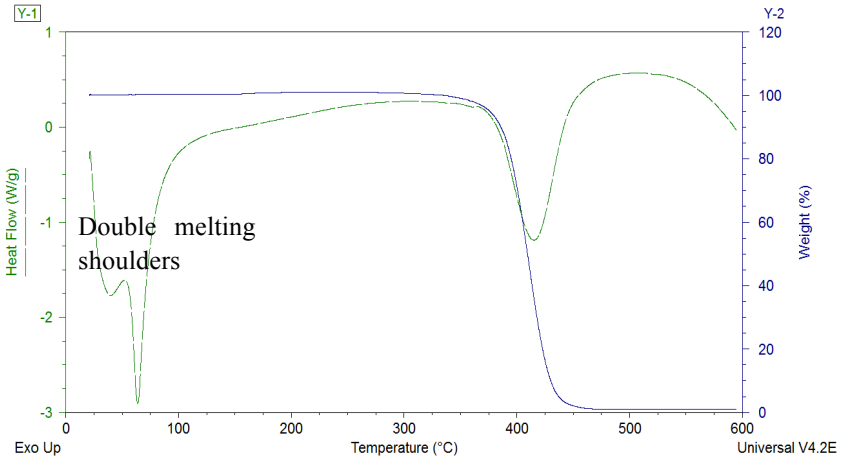

Figure 5 - SDT analysis exemplifying typical double melting shoulders.

The melting temperature and enthalpy results, for pure and for $scCO_2$-foamed PCL and PCL/MCM-41 samples are presented in Figure 6. While the supplier reports melting temperature values around ~56-64 ºC (for this molecular weight), SDT results indicated different and higher values (~67-68 ºC). Considering the indicated standard deviations, no apparent change occurred in the melting temperatures of PCL pellets and powder. PCL $scCO_2$-assisted processing lowered the melting temperature when compared with unprocessed samples. This effect becomes more pronounced (~65 ºC) for the higher processing pressure (25 MPa). It is important to notice that contradictory results on the processing pressure effects in PCL melting temperatures can be found in literature: while some authors refer that melting temperatures were lowered by higher processing pressures (Shieh *et al.*, 2005, Tsivintzelis *et al.*, 2007), others refer the opposite trend (Kiran *et al.*, 2008, Salerno *et al.*, 2011). Furthermore, the aforementioned typical endothermic peaks, were also changed (from ~47 ºC down to ~37 ºC). This indicates that PCL underwent crystallization (Kiran *et al.*, 2008), and that the process decreased the crystallinity (Shieh *et al.*, 2009, Léonard *et al.* 2008, Jenkin 2007, Shieh *et al.* 2005, Kiran *et al.*, 2008), contrarily to what was reported by other researchers (Jenkins *et al.* 2006, Xu *et al.* 2004). Melting enthalpies are majorly influenced by MCM-41 content, which may be also suggestive of the crystallinity state. Thus, it can be observed that, maintaining silica content constant, the enthalpies for samples processed at different pressures vary only a few. However, increasing MCM-41 content the melting enthalpy decreases, due to lack of intercalation between the polymer and the inorganic element. Between pellet and powder PCL the difference is considerable which can be assigned to the increase in crystallinity upon the powder formation. Finally, and despite the obtained standard deviations, the incorporation of MCM-41 SNPs during the $scCO_2$ processing also seems to induce a further decrease in PCL melting temperature (Salerno *et al.* 2011): at 14 MPa the temperature decreases from ~67ºC to ~65ºC and at 25 MPa the reduction from ~65ºC to ~64ºC.

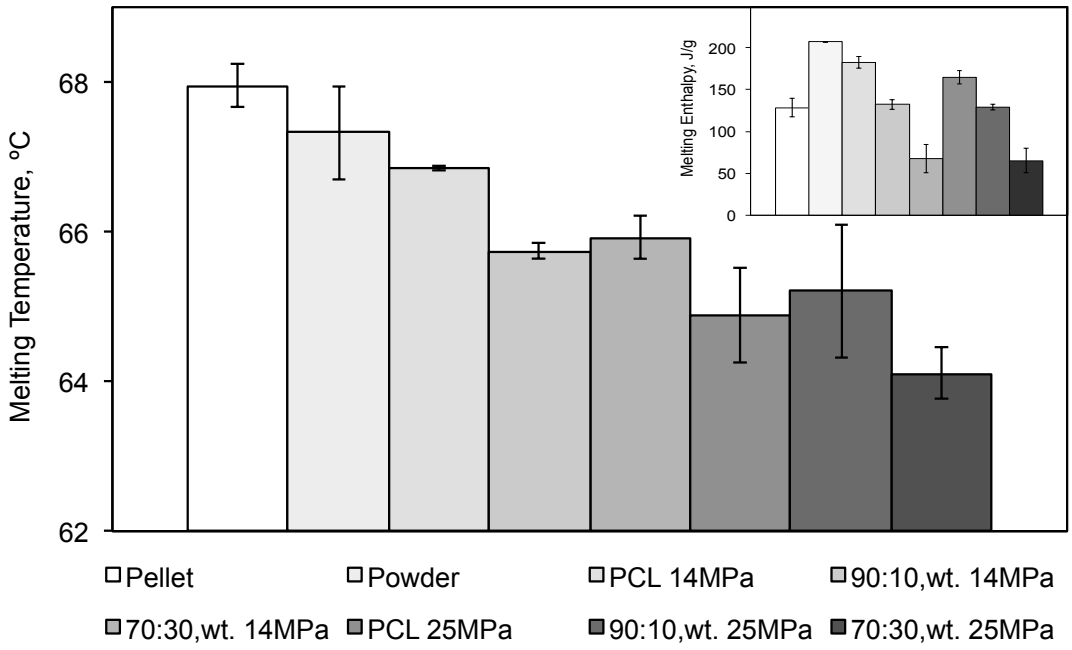

Figure 6- Melting Temperature and Enthalpy of PCL and its composites processed for 2 h and 3.0 L/min.

PCL degradation temperatures (Figure 7) remain almost constant for all processed samples despite a decrease in these values can be observed for samples containing higher MCM-41 SNPs amounts. The degradation enthalpies present the same behavior of the melting enthalpies, but the energy involved in the degradation of one gram of sample is larger. Therefore, thermally induced degradation seems to be favored by the presence of SNPs.

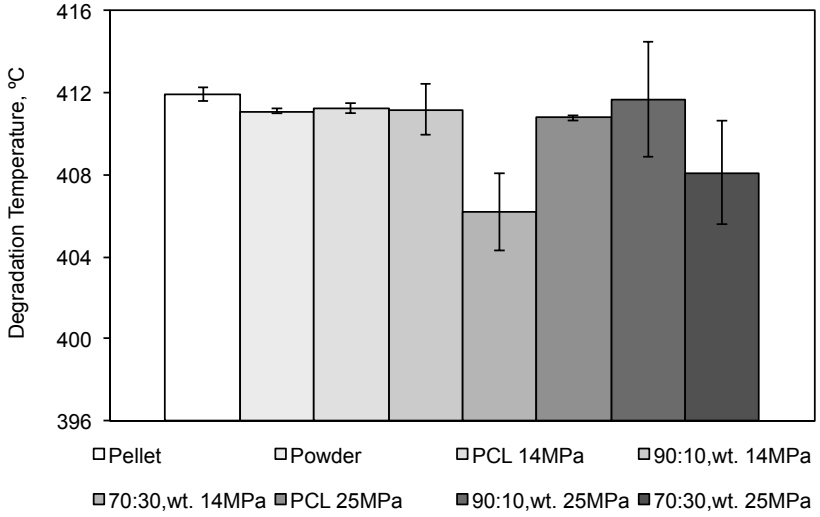

Figure 7 - Degradation Temperature of PCL and its composites processed for 2 h and 3.0 L/min.

In general, higher melting/degradation temperature corresponds to higher crystallinity. Therefore, XRD was performed in order to confirm the crystallinity conclusions. Figure 8 shows the XRD patterns of PCL (pellet and powder), PCL processed at 14 and 25 MPa (14h and 3L/min) and 70:30,wt.% (14h and 3L/min). Non-processed and processed pure PCL samples show little differences in

crystallinity (as previously seen in SDT results), thus the resultant d-spacing, width at half-heights and peak areas are similar. Crystallinity also varied induced by pressure: for lower pressure the polymer matrix organization is higher. Polymer melting and subsequent foaming at this condition occurs in lower extent than at higher pressures, leading to a material with thermal and crystallinity properties similar to the original polymer. As also predicted from SDT analysis, the processed 70:30,wt.% composite crystallinity clearly decreased, given that the peaks area decreased and the peaks are broader. Similar XRD results were obtained for other processing conditions and these results are in good agreement with the previously discussed SDT results.

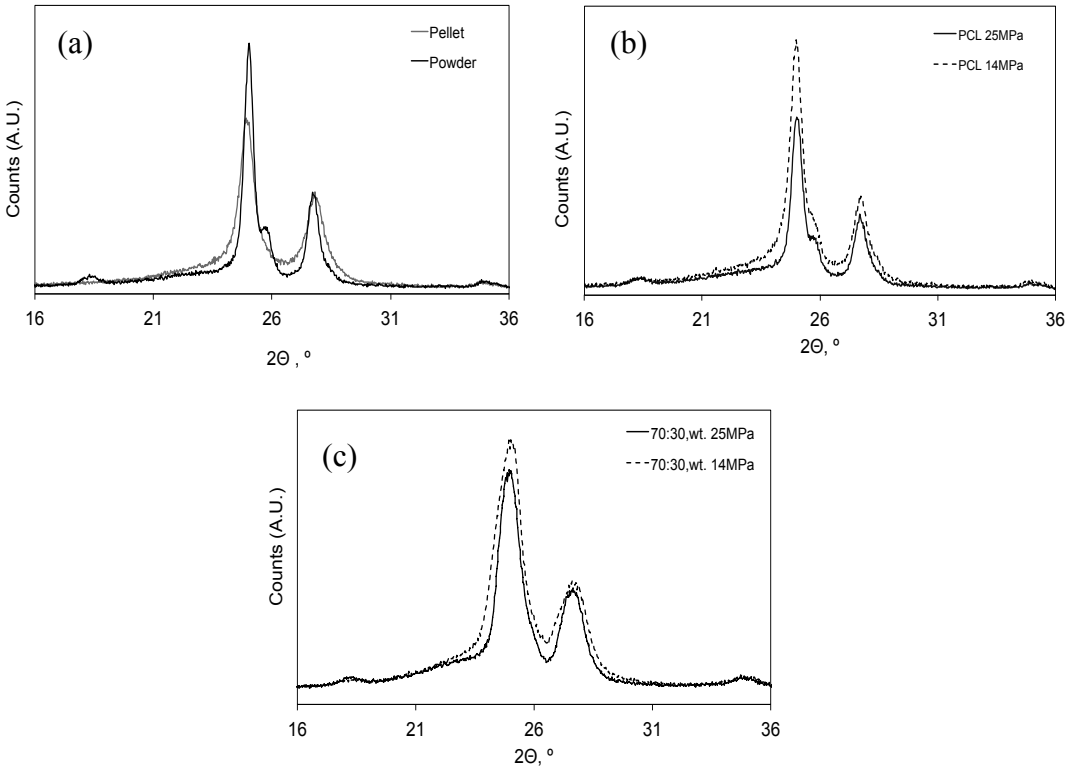

Figure 8 - XRD Patterns of (a) PCL pellet and powder, (b) PCL and (c) composite 70:30,wt.% processed at 14 and 25 MPa for 14h, 3.0 L/min.

Disagreement often found in literature regarding the final morphology of polymeric foams, is due to countless factors involving supercritical-assisted foaming. Morphology will express the arrangement state: amorphous and unordered or crystalline and ordered. Crystalline polymers are either able to form thin and plate-like lamellar structures when crystallization occurs from solutions, or when crystallized from melt they can form stacks of lamellar structures (spherulites) (Kiran, 2008).

The molecular structure and initial crystallinity and the polymer:$scCO_2$ ratio (which defines the $scCO_2$ solubility in the polymer) will determinate how much CO_2 can be dissolved in the polymer (Fanovich *et al.* 2012). Also, the process parameters (temperature, pressure, time and depressurization rate) have influence in this subject. As explained in Section 1.2.1, $scCO_2$ penetrates the amorphous phase due to increased gas dissolution; plasticization of the amorphous region increases the mobility of the

polymeric chains, which enables them to rearrange, induces crystallization and related changes in morphology (Jenkins, 2007). Hence, if the initial polymer crystallinity, molecular weight and mass are high, the amount of CO_2 required to be dissolved in the polymer would be also higher. Therefore, higher saturation pressure/temperature/process time would be necessary. As mentioned by Fanovich and co-workers (2012), at high pressure the polymer is able to uptake more gas and the studied systems, at 35ºC and 20 MPa PCL was completely melted after 20 min, but at 15 MPa (and same temperature) melting occurs only after 50 min.

In this sense, the dissolution strength, in the case of dense fluids, is increased as the pressure is increased because the lower critical solution temperature (LCST) and upper critical solution temperature (UCST) are shifted to higher and lower temperatures, correspondingly. Also, as the fluid sorption occurs, the T_c and T_g are lowered from their initial values (Kiran, 2008, Kiran *et al.*, 2008). At a constant temperature, the supercritical solution starts to be formed and the polymer composition moves from 100% polymer to lower polymer concentration. At this composition and increasing the pressure, the system would increase the equilibrium crystallization temperature and as long as these Pressure/Temperature conditions are not enough to take the polymer above its T_c curve, the rearrangements transformations will occur in the S-L boundary. When increasing pressure the concentration of the polymer lowers to even lower polymer concentration, and the T_c is lower than it was for the previous case. According to Kiran *et al.* (2008) the increased pressure promotes crystal rearrangement and, for the system studied by this author, at 21MPa and 35ºC the system remains below its equilibrium T_c curve and the crystal rearrangement happens in the solid state (Kiran *et al.*, 2008).

However, when depressurization is induced, the system tends to move towards 100%polymer composition and the result is a polymer with variable lamellar thickness and thus variable melting temperatures, depending not only on the initial (P,T) conditions, but also on the depressurization paths (Kiran *et al.*, 2008). At constant pressure and temperature, rapid depressurization would lead to organized crystals, while slow depressurization would in turn lead to less organization of the crystalline net. Typical depressurizations found in literature range from 2s to a few minutes while in this work it ranged from 10 min to several hours; nevertheless, the results obtained in this work are in agreement with literature. Low depressurization rate leads to less organized structures and the melting temperature (that can give information about the crystalline state) lowered (not represented).

The same author referred that the crystallization process only stops when the T_g is reached with a further cooling step, which may occur by Joule-Thompson effect. If the temperature is low for low polymer composition the system may go through L-L phase separation and crystallization would occur only with further cooling. For higher temperatures the system carries crystallization crossing S-L boundary, never entering the L-L phase separation domain. When higher pressures are induced, the LCST and UCST separation is broader, and when the temperature is lowered, the L-L boundary

is never crossed. In this case, even for the lowest polymer concentration, crystallization occurs as it was taken from melt at ambient pressures (Kiran 2008, Kiran *et al.*, 2008). Thus, lower melting temperature of the thinner lamellar structures will rise in contrast to melting at lower temperatures (Kiran *et al.*, 2008).

Concluding, upon depressurization, if the initial pressure and temperature is low (as in the case of this work, 35ºC) the system may cross the L-L boundary and the crystalline phases may not be formed at the same extent, as they would be if the initial temperature/pressure were higher.

Additionally, the method used to mix polymeric and inorganic phases affect the morphology of the final composite (Lee *et al.*, 2005). The typical method for mixture is compression molding and the one used was the simple physical mixture of two powders. In this case, the existence of more voids is higher and MCM-41 will act as an impurity, because of the lack of intercalation within the polymer phase (Smith *et al*., 1998). Likewise, PCL particle size will matters for this subject: the bigger the particles the less proximity would exist between inorganic and polymer, and the less intercalated both components would be at the end of the process. Thus, the melting and degradation temperatures of the final product will tend to decrease with increasing filler content, as seen in this work. However, melting and degradation temperatures obtained are above the body temperature, making these materials suitable for biomedical applications.

3.2. Polymer and Composites Morphology

3.2.1. Density and Porosimetry

Macroscopic analysis reveals differences between the employed working conditions and the influence of MCM-41 content, as it can be observed in Figure 9. For the same mass, as the inorganic content is decreased the volume also decreases, which means that the porosity decreases. Pressure increase leads to an increase of samples volume, which can also indicate that the overall porosity is higher. Also, decreasing the depressurization rate leads to an apparent increase of sample volume.

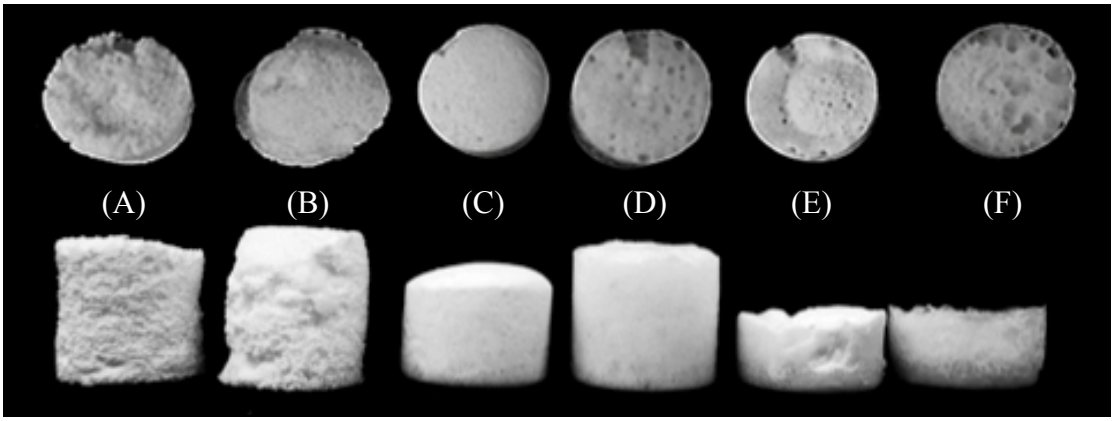

Figure 9 – Samples processed at different conditions. 70:30,wt.% 14MPa 3L/min (A), 70:30wt.,% 25MPa 0.2L/min (B), 90:10,wt.% 14MPa 3L/min (C), 90:10,wt% 25MPa 0.2L/min (D), PCL 14MPa 3L/min (E) and PCL 25MPa 0.2L/min (F)

In order to further investigate the accuracy of the macroscopic results, pore size, density and porosity were obtained by nitrogen adsorption, helium picnometry and mercury intrusion are also presented in Tables B1-B3 in Appendix B.

Nitrogen Adsorption

Regarding surface area, this result is mostly dependent on silica content and pressure, as revealed in Figure 10. Higher amounts of SNPs and higher pressure led to higher surface areas. Surface area also tends to increases with processing time, and depressurization rate. Therefore, samples 70:30,wt.% have the larger surface area (from 20.5 m^2/g to 11.2 m^2/g when processed at 14 MPa, and from 134.7 to 17.5 m^2/g when processed at 25 MPa) (Figure10A); 90:10,wt.% samples show intermediate surface area values: at 14 MPa its range is 1.3 m^2/g up to 1.9 m^2/g, and using processing pressure of 25 MPa, surface area varies between 39.6 m^2/g and 1.3 m^2/g (Figure 10B). Foamed PCL shows much lower values of surface area, between 0.5 m^2/g and 0.9 m^2/g, and it seems constant for all tested operational parameters (Figure 10C).

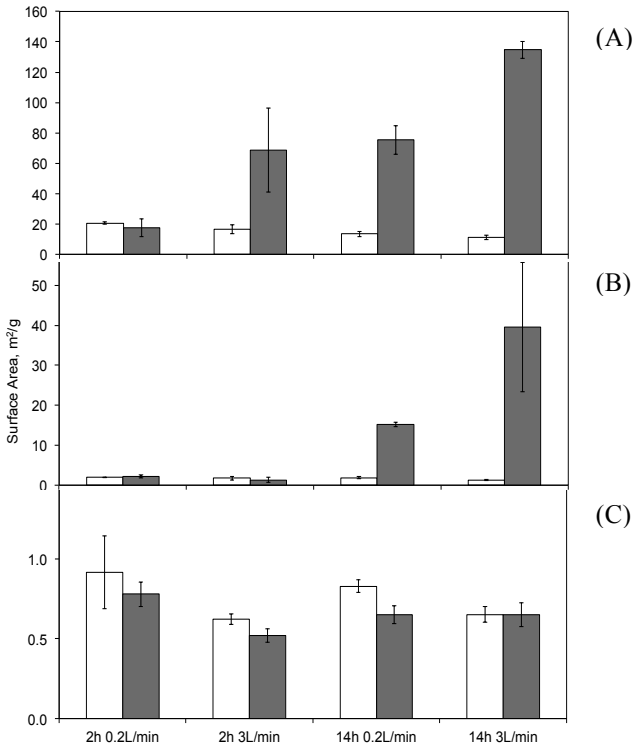

Figure 10 - Surface Area (m^2/g) of samples processed at 14 MPa (□) and 25 MPa (■): 70:30,wt.% (A) 90:10,wt.% (B) and PCL (C).

Samples pore volumes were also found to increase with the increasing silica content and pressure. These results are disclosed in Figure 11. Processing time and depressurization rate don't significantly influence this property: processing time

increase led only to a slight increase in pore volume and rapid depressurization led to increase of pore volume except for 100wt.% PCL samples. Therefore, the samples showing the largest pore volumes are those of 70:30,wt.%, as shown in Figure 11A (40.0±2.1x10^{-3} cm^3/g at 14 MPa, and 151.0±51.5x10^{-3} cm^3/g at 25 MPa), followed by 90:10,wt.% (Figure 11B). PCL samples showed the lowest and almost constant values (Figure 11C), which were between 1.8±0.2x10^{-3} cm^3/g and 1.4±0.5x10^{-3} g/cm^3 (at 14 MPa) and for higher pressure this range was from 1.6±0.1x10^{-3} cm^3/g to 0.9±0.4x10^{-3} cm^3/g.

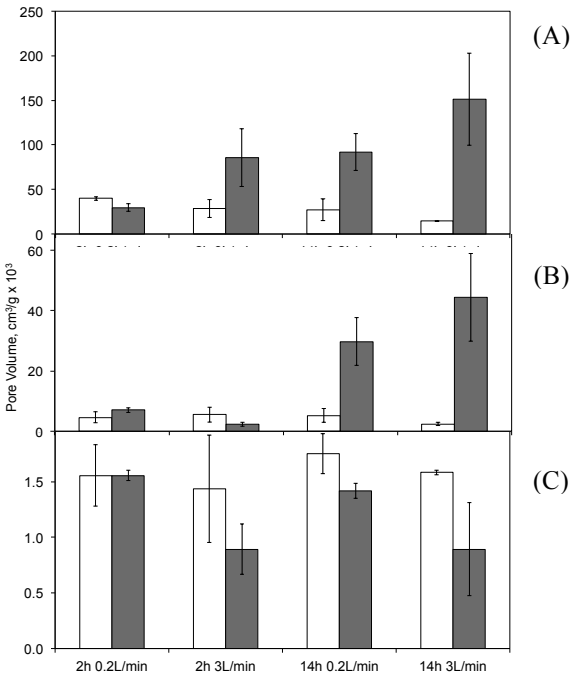

Figure 11 - Pore volume (cm^3/g) of samples processed at 14 MPa (□) and 25 MPa (■): 70:30,wt.% (A) 90:10,wt.% (B) and PCL (C).

Another physical parameter assessed by nitrogen adsorption was the average pore diameter. In Figure 12 is possible to observe that rapid depressurization and higher pressure led to a decrease of pore diameter while processing time had no clear effect on pore diameter (Figure 12A-12C). Increasing silica content increased pore diameter up to a certain amount of SNPs (10%); above this silica composition pore diameter value decreased, as it can be observed in Figure 12D. Thus, PCL and 70:30,wt.% samples show the smallest pore diameters, from 53.8 to 96.6 Å and from 46.5 to 111.8 Å, respectively.

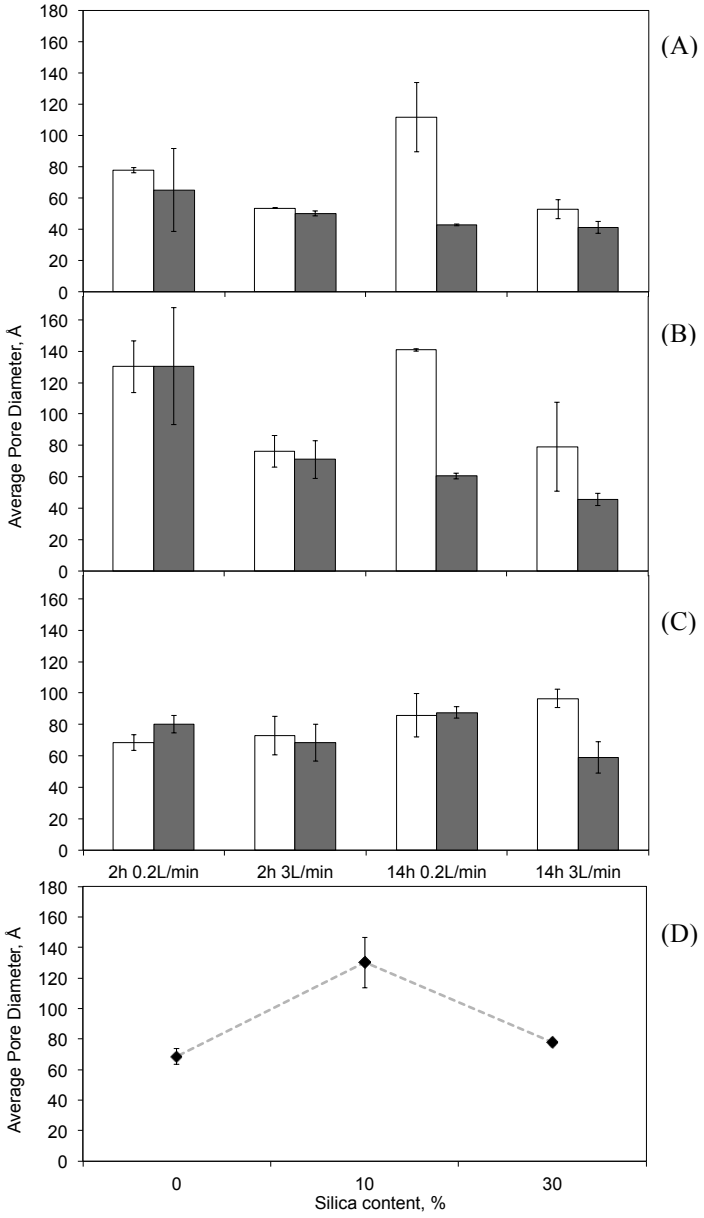

Figure 12 - Average pore diameter (Å) of samples processed at 14 MPa (□) and 25 MPa (■): 70:30, wt.% (A) 90:10 ,wt.% (B) and PCL (C). Silica content influence on average pore diameter for samples processed at 14 MPa, 2h and 0.2L/min (D).

Samples subjected to higher pressure (Tsimpliaraki *et al.*, 2011, Kiran, 2010, Tai *et al.*, 2007), processing time (Tai *et al.*, 2007), and rapid depressurization (Jenkins *et al.*, 2006, Kiran, 2010, Tai *et al.*, 2007) usually show lower average pore diameters. In section 1.2.1 the homogenous and heterogeneous nucleation theories were briefly explained: for higher pressures the generation of the initial bubble nuclei is favored, and this will dictate the final pores formation. Increasing pressure will also increase CO_2 solubility in the polymer matrix and more supercritical solvent is available for pore nucleation. As a consequence of the necessity to distribute the available CO_2 to all the new-formed nuclei, smaller pores are formed (Tsimpliaraki *et al.*, 2011). Tai *et al.* (2007) and Xu at al. (2004) refer that, in addition to higher pressure, longer process times would allow more opportunity to more CO_2 molecules to diffuse into

the polymer, but this effect was not verified. Increasing the inorganic content up to 10% also increases the average pore diameter as reported by Lee *et al.* (2005) and Collins *et al.* (2008), but contrarily to Tsimpliaraki *et al.* (2011), who described that smaller pores are obtained as more silica is added. The latter author, Zhai *et al*. (2006) and Collins *et al*. (2010) also reported that the increase in silica amount leads to more pores and reduction of pore size distribution. Finally, considering the inorganic filler, the presence of SNPs will favour heterogeneous nucleation: the accumulation of gas on the polymer/particle interface will create nucleation sites (Lee *et al.*, 2005) and thus more and smaller pores, with lower inter-pore separation, will be formed (Collin *et al.*, 2010). This happens because the absence of SNPs stimulates formation of pores in a random manner and its addition offers extra sites for nucleation to happen (Collins *et al.* 2008) and lowers the energy barrier for pores formation. Thus, the reduction of the pore size distribution is enhanced (Collins *et al.*, 2008). Regarding depressurization rate, Collins *et al*. (2010), Jenkins *et al*. (2006), Xu *et al*. (2004), Kiran (2010) and Tai *et al*. (2007), stated that lower depressurization rates allow the formation of larger pores in the final construct. This effect is due to the gas diffusion rate in the liquefied polymer (which is determined by the viscosity of the solution), which was observed in most cases.

Adsorption-desorption isotherm type 4 curve was found in all samples, which is revealing of adsorbents with relatively large pores. This behavior is normally attributed to mesoporous (pores greater than 20 Å) or macroporous (pores larger than 500 Å) materials, which are likely to present a wide range of pores shapes and sizes which may also be interconnected with one another (Webb *et al*., 1997).

Helium picnometry

Figure 13 shows that samples density is mainly affected by the inorganic filler amounts, and as such, the increasing MCM-41 SNPs content led to higher density for all tested conditions. Increasing pressure slightly augments the density in 70:30,wt.% and 90:10,wt.% samples. Processing time and depressurization rate seem to have no strong effect on final sample density.

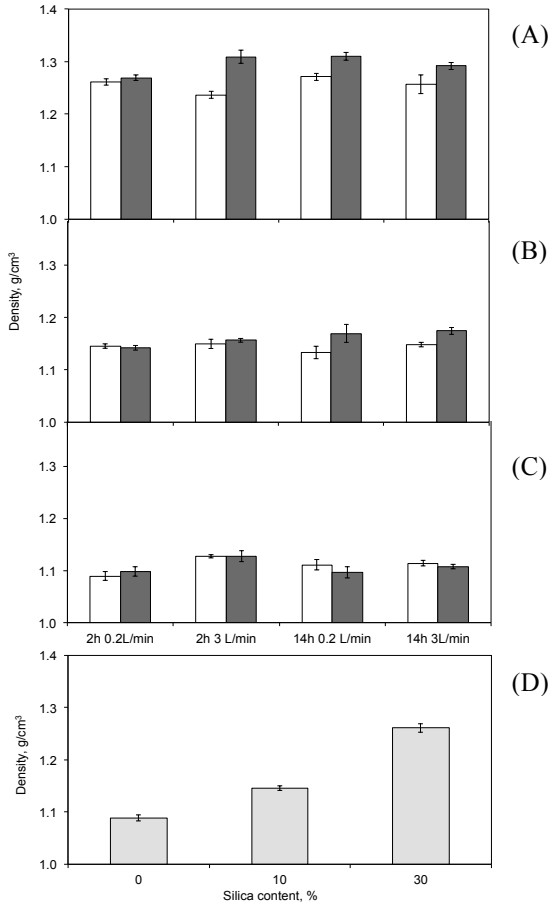

Figure 13 – Density (g/cm^3) of samples processed at 14 MPa (□) and 25 MPa (■): 70:30, wt.% (A) 90:10 ,wt.% (B), PCL (C). Influence of silica content in density for samples processed at the same conditions (14 MPa, 2h, 0.2L/min) (D).

Mercury intrusion

Porosity, density and average pore diameter were determined by mercury intrusion. Density results are similar to those formerly obtained by nitrogen adsorption and for that reason they are not showed here. Regarding porosity, the major variable that affects this property is MCM-41 content (Figure 14); higher SNPs amounts confer more nucleation points during depressurization, which leads to higher porosity. Pressure, on the other hand, does not have a clear effect, but the tendency is to slightly decrease the porosity with increasing pressure (Figure 14A). Longer processing time tends to increase porosity (Figures 14B and 14C) once CO_2 sorption and polymer melting is enhanced for higher process times (Fanovich *et al.*, 2012). Depressurization rate (Figures 14D and 14E) seems to have no influence on the porosity of 70:30,wt% composites but for 90:10,wt% and PCL foams (and both pressures) increasing depressurization rate led to a decrease in porosity. This effect can be explained by the coalescence of neighboring newly formed pores: the CO_2 rapidly leaves the material matrix leaving pores behind, but the material tends to aggregate again because it had few time to rearrange. Nevertheless, and as it can be confirmed in Table B2, the

highest porosity value was found for 70:30,wt% samples processed at 25 MPa (55.4±0.3%) and the lowest was for PCL samples processed at the same pressure (11.9±1.7%). 90:10,wt% composites show, once again, intermediate values between 50.4±5.9 % (at 25 MPa, Figure 14C) and 16.4±1.0% (at 14 MPa,).

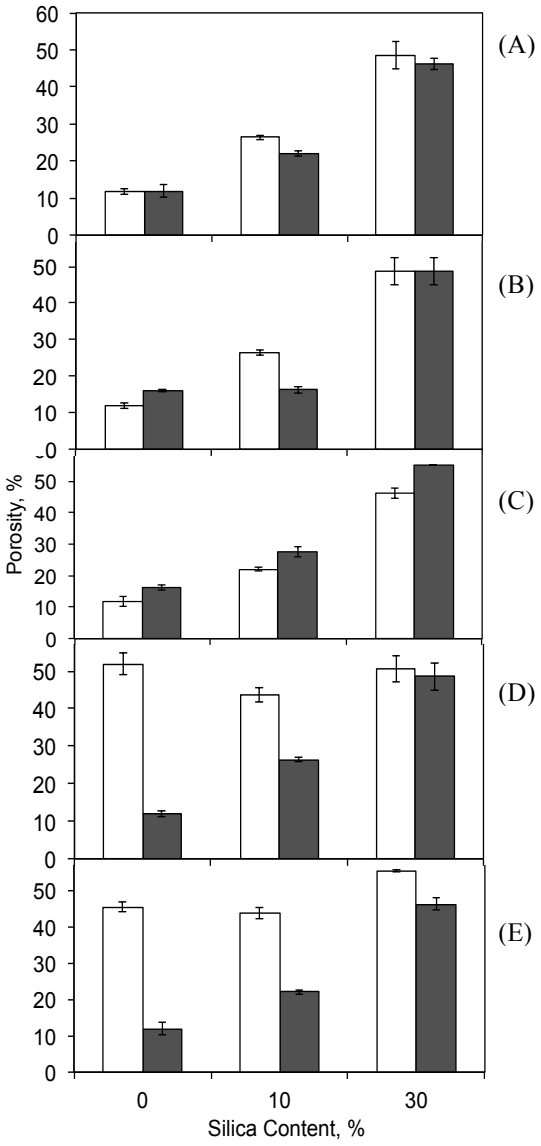

Figure 14 – Porosity (%) variation with the employed conditions: Effect of pressure at 2h and 3.0 L/min □ 14 MPa ■ 25 MPa (A). Effect of time at 14 MPa (B) and 25 MPa (C) and 3L/min □ 2 h and ■ 14 h. Effect of depressurization rate at 14 MPa (D) and 25 MPa (E) and 2h □ 0.2 L/min and ■ 3.0 L/min.

Obtained average pore diameters are represented in Figure 15. Increasing pressure does not have a clear effect on this property (Figure 15A), and pores tend to increase their size when longer process time is employed. In the latter case (processing time), the only exception concerns 90:10,wt%, were the diameter is practically constant (Figures 15B and 15C). The most obvious effects are the depressurization rate and SNPs amount. Smaller pores are found when higher inorganic content and the depressurization rate are employed (Figures 15D and 15E).

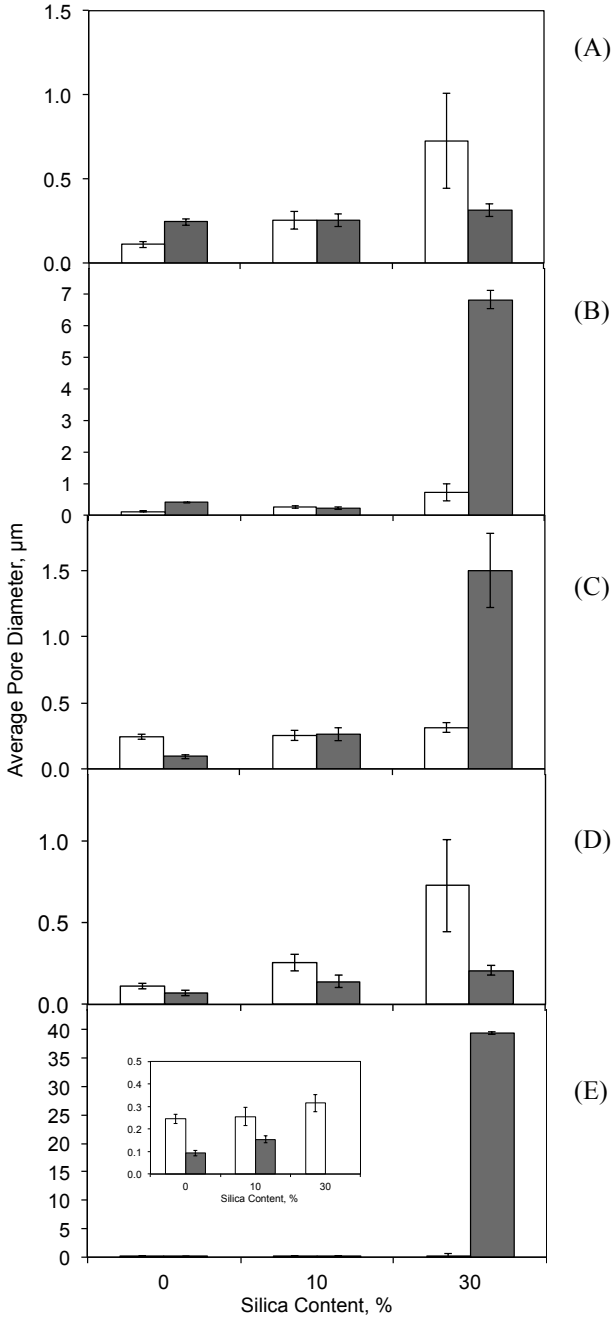

Figure 15 - Average pore diameter (µm) variation with the employed conditions: effect of pressure for 2h and 3.0 L/min □ 14 MPa ■ 25 MPa (A). Effect of time for 0.2 L/min at 14 MPa (B) and 25 MPa (C) and □ 2 h ■ 14 h. Effect of depressurization rate for 2h at 14 MPa (D) and 25 MPa (E) □ 0.2 L/min ■ 3.0 L/min. In Figure (E) it is possible to see with the detail of the lower values.

When higher amounts of MCM-41 SNPs were introduced into PCL (30 wt.%), pore sizes seem to decrease again. MCM-41 SNPs will act as nucleating agents for the forming gaseous CO_2. Moreover, the distribution of these nucleating agents (which is determined by the efficiency of the method employed to mix polymeric and inorganic phases) will dictate the number and the sizes of the final pores (Lee *et al*., 2005). As more SNPs are introduced, more nucleation points will be created and thus the number of growing bubbles will be larger (for the same amount of dissolved $scCO_2$). Nevertheless, their resulting dimensions will be smaller (Tsimpliaraki *et al*. 2011, Zhai *et al.*, 2006).

3.2.2. Scanning Electron Microscopy

The morphology of the supercritical processed material was explored as well by SEM and the results are presented in Figures 16 and 17.

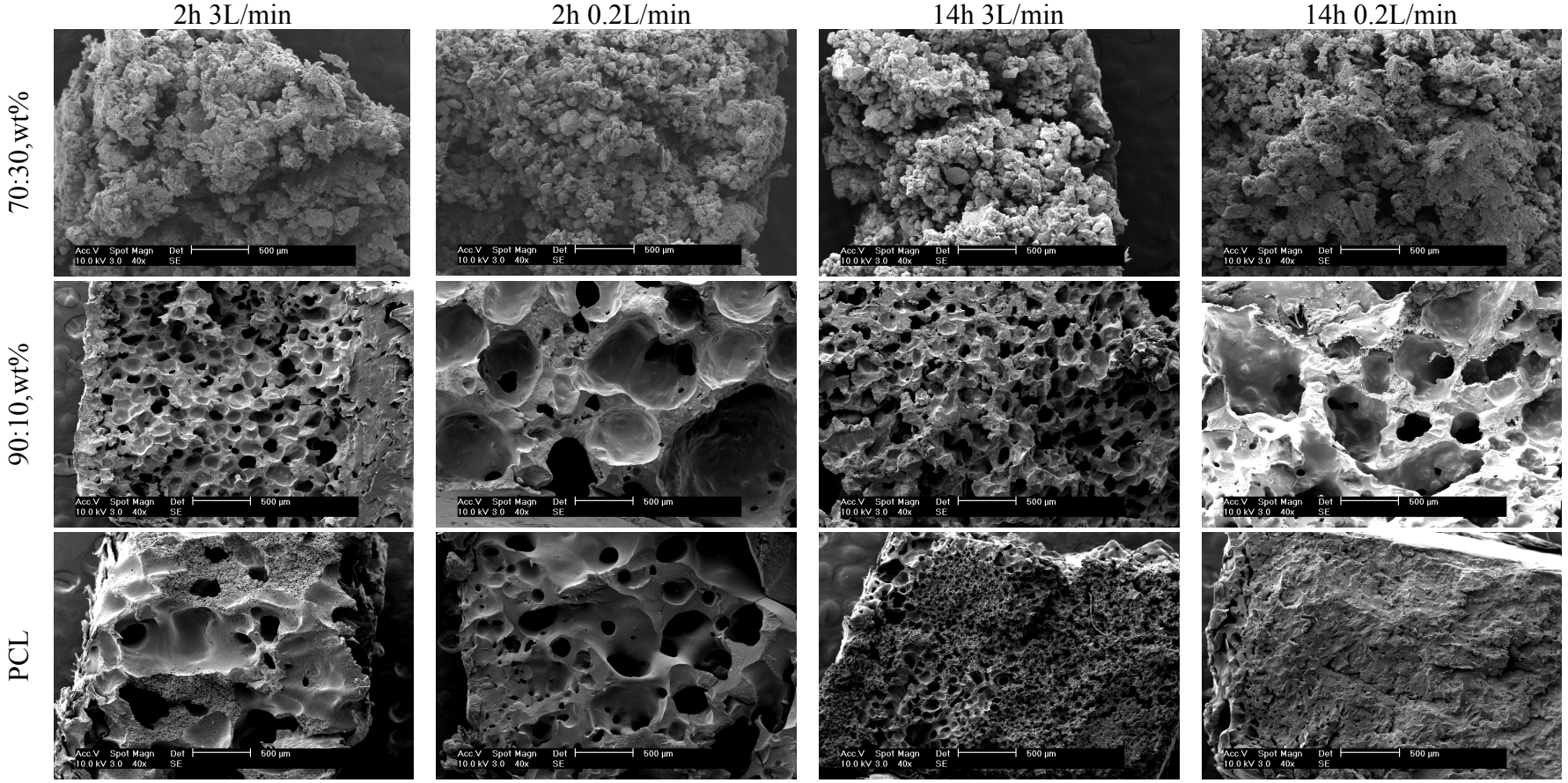

Figure 16 - SEM of samples processed at 14MPa. Magnification 40x. Scale bar 500 µm.

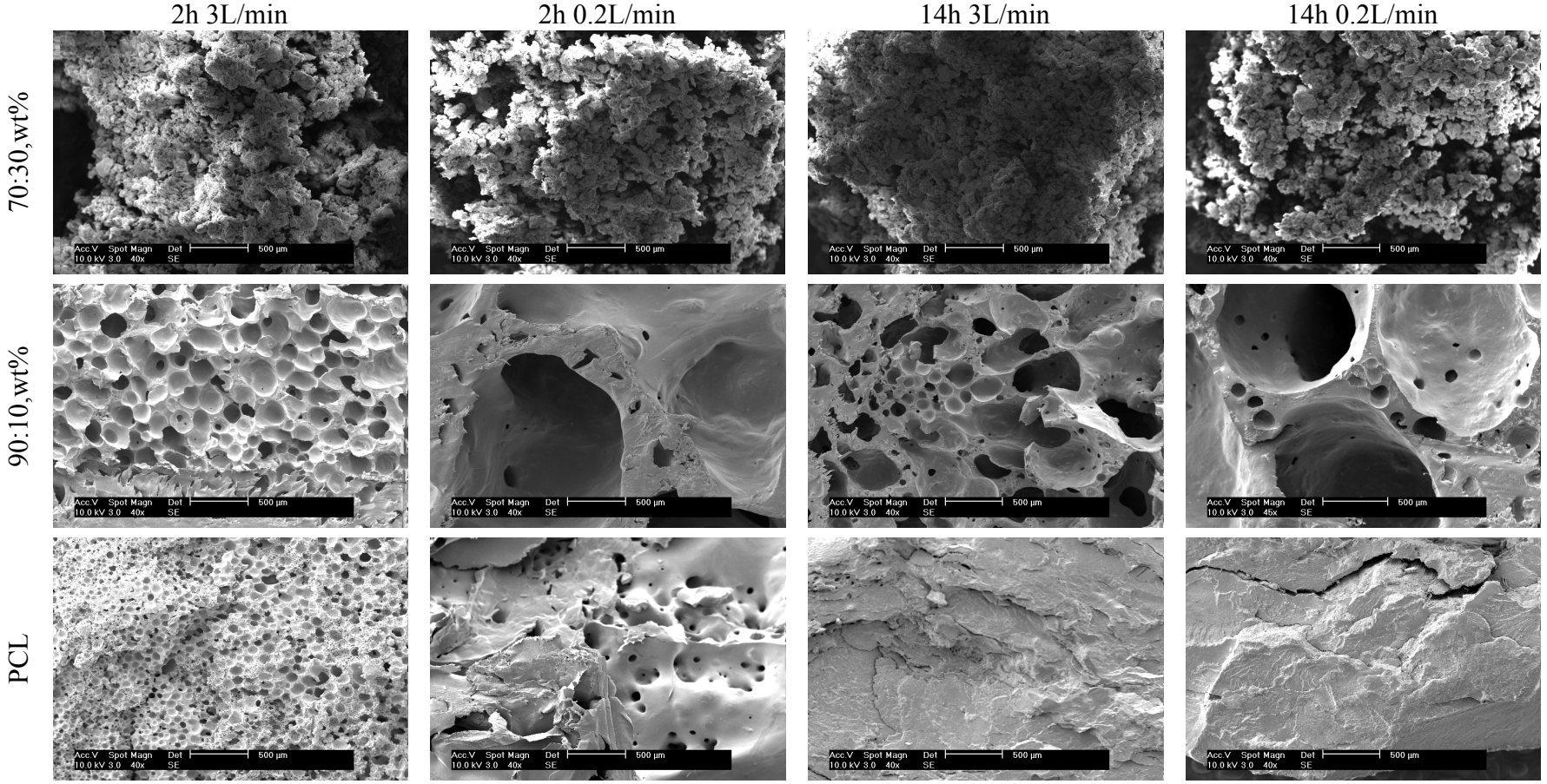

Figure 17 - SEM of samples processed at 25MPa. Magnification 40x. Scale bar 500 μm.

It can be observed by SEM pictures (Figures 16 and 17) that different process conditions originated distinct porous morphologies. In general the tendency described previously was verified: increasing silica content increased pore diameter up to a certain amount of SNPs (10%) and above this silica composition pore diameter value decreased.

In 70:30,wt% samples we are not able to see pores due to the extremely small size; in 90:10,wt% material is possible to observe pores with diameters from approximately 50 μm up to pore diameters higher than 500 μm. PCL processed material presents pore diameters that can be from also tens of micron up to 500 μm, while in some cases, for the presented magnification, it seams that there are no pores but these can be inferior to 20 μm, as represented in Appendix C.

The results can be attributed to several aspects that concern the samples preparation for the latter methods and to different morphology that can occur in different places of the same sample. For nitrogen adsorption and mercury intrusion the preparation of the samples required them to be cut in thin pieces with 0.5 mm (or less) of diameter, which would exclude the analyses of pores bigger than this. On the other hand, the morphology of these type of materials maybe variable according to the location; for this reason, the sampling to SEM was made from one slice on the central region of the samples.

Observing the pictures and gathering information acquired by nitrogen adsorption and mercury intrusion, it is possible to achieve wide range of pore sizes and morphology that are suitable for new tissue formation.

3.3. Texturometry

Foam architecture is known to have an effect on foam mechanical resistance and for that reason PCL and its composites were tested for compression. Results are represented in the Table 2 and Figures 18-20. Variations in mechanical resistance can be observed mostly due to the filler content, in disagreement with Georgiou *et al.* (2006) but in agreement with Mathieu *et al.* (2005), and the obtained results, specially for 90:10,wt.% samples, are similar to previous studies with other composite materials, such as PLA/phosphate glass, PLA/β-TCP, and PLA/HA (Georgiou *et al.*, 2006, Mathieu *et al*., 2005, Lee *et al.*, 2005). A linear elastic region was visible (and used to determine the compressive modulus) previous to the plateau.

Table 2 - Stress and Compressive Modulus of all the samples processed by $scCO_2$ foaming.

Sample			Stress, MPa (at 10% Strain)	Compressive Modulus, MPa
70:30,wt.%	2h 14MPa	3L/min	2.30 ± 0.23	20.29 ± 5.66
		0.2L/min	1.51 ± 0.91	11.35 ± 7.12
	14h 14MPa	3L/min	7.44 ± 4.23	65.71 ± 35.32
		0.2L/min	5.66 ± 1.84	47.14 ± 27.42
	2h 25MPa	3L/min	4.12 ± 0.55	30.85 ± 6.90
		0.2L/min	4.50 ± 2.06	29.36 ± 17.66
	14h 25MPa	3L/min	2.50 ± 1.70	21.59 ± 10.83
		0.2L/min	3.65 ± 1.67	29.01 ± 18.16
90:10,wt.%	2h 14MPa	3L/min	17.47 ± 1.60	164.39 ± 9.52
		0.2L/min	17.40 ± 0.44	131.75 ± 1.06
	14h 14MPa	3L/min	8.89 ± 5.00	171.12 ± 0.00
		0.2L/min	14.88 ± 5.78	77.47 ± 1.97
	2h 25MPa	3L/min	13.88 ± 1.46	138.41 ± 46.27
		0.2L/min	17.00 ± 4.10	131.31 ± 18.38
	14h 25MPa	3L/min	10.22 ± 5.21	60.43 ± 29.98
		0.2L/min	15.88 ± 2.51	124.34 ± 8.52
PCL	2h 14MPa	3L/min	4.39 ± 0.17	32.19 ± 2.13
		0.2L/min	2.05 ± 0.09	20.24 ± 0.62
	14h 14MPa	3L/min	2.10 ± 0.20	22.17 ± 0.83
		0.2L/min	4.12 ± 3.20	40.11 ± 31.86
	2h 25MPa	3L/min	3.17 ± 2.76	24.61 ± 17.08
		0.2L/min	2.23 ± 1.00	23.29 ± 11.20
	14h 25MPa	3L/min	2.09 ± 0.29	20.23 ± 6.63
		0.2L/min	2.58 ± 0.13	27.49 ± 3.34

The mechanical compression results were calculated at a 10% strain, and suggest that higher compressive stress (from 15.9±2.5 to 8.9±5.0 MPa) and moduli (164.4±9.5 to 60.4±29.9 MPa) were obtained for samples containing an intermediate amount of SNPs (10%), despite the processing conditions. However, these values are still inferior to trabecular bone, which presents compressive modulus of approximately 0.3 GPa (Baker *et al*. 2009, Georgiou *et al.* 2006). The 70:30,wt.% samples exhibit unsuitable mechanical properties and heterogeneities that are visible by the standard deviation errors. Also, PCL samples reveal values inferior than 90:10,wt.%, but still appropriate for load bearing applications (Lee *et al.*, 2005, Zhai *et al.*, 2006).

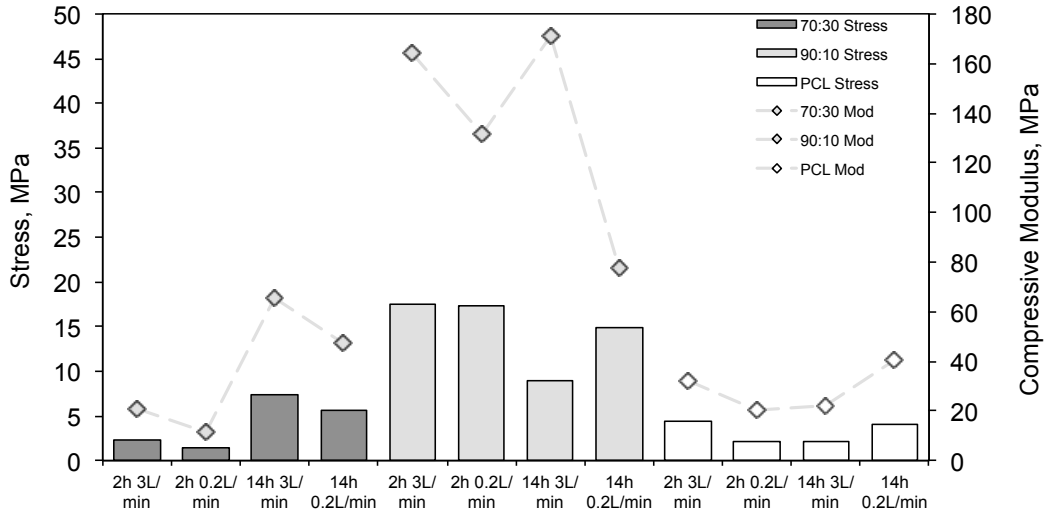

Figure 18 – Stress (at 10% of strain) and Compressive Modulus of PCL and PCL/MCM-41 composites processed at 14 MPa.

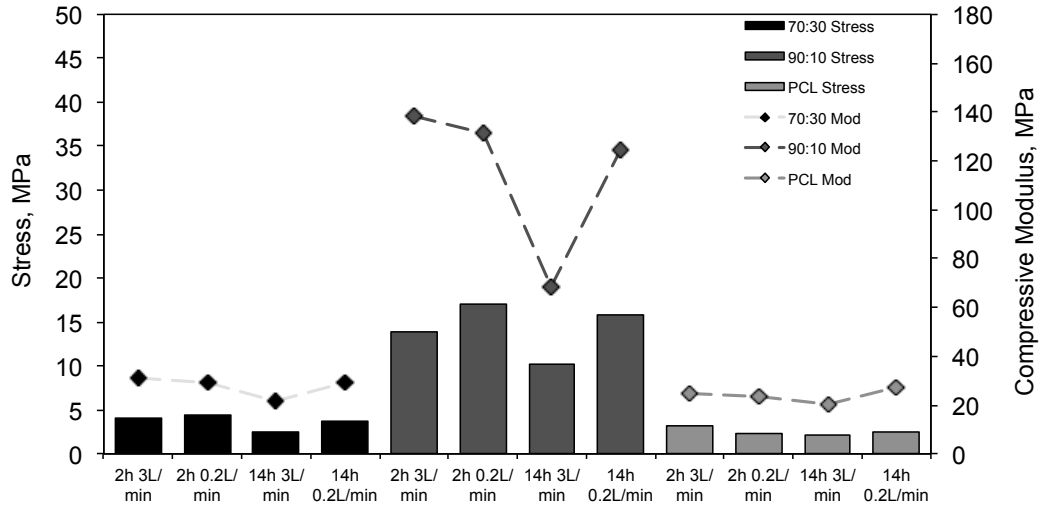

Figure 19 - Stress (at 10% of strain) and Compressive Modulus of PCL and PCL/MCM-41 composites processed at 25 MPa.

According to model of Gibson and Ashby (Mathieu *et al.*, 2005) both moduli and stress decrease with increasing porosity; in this work this tendency was confirmed in almost all samples, as it is exemplified in Figure 20, and the exceptions can be explained by heterogeneities of the material.

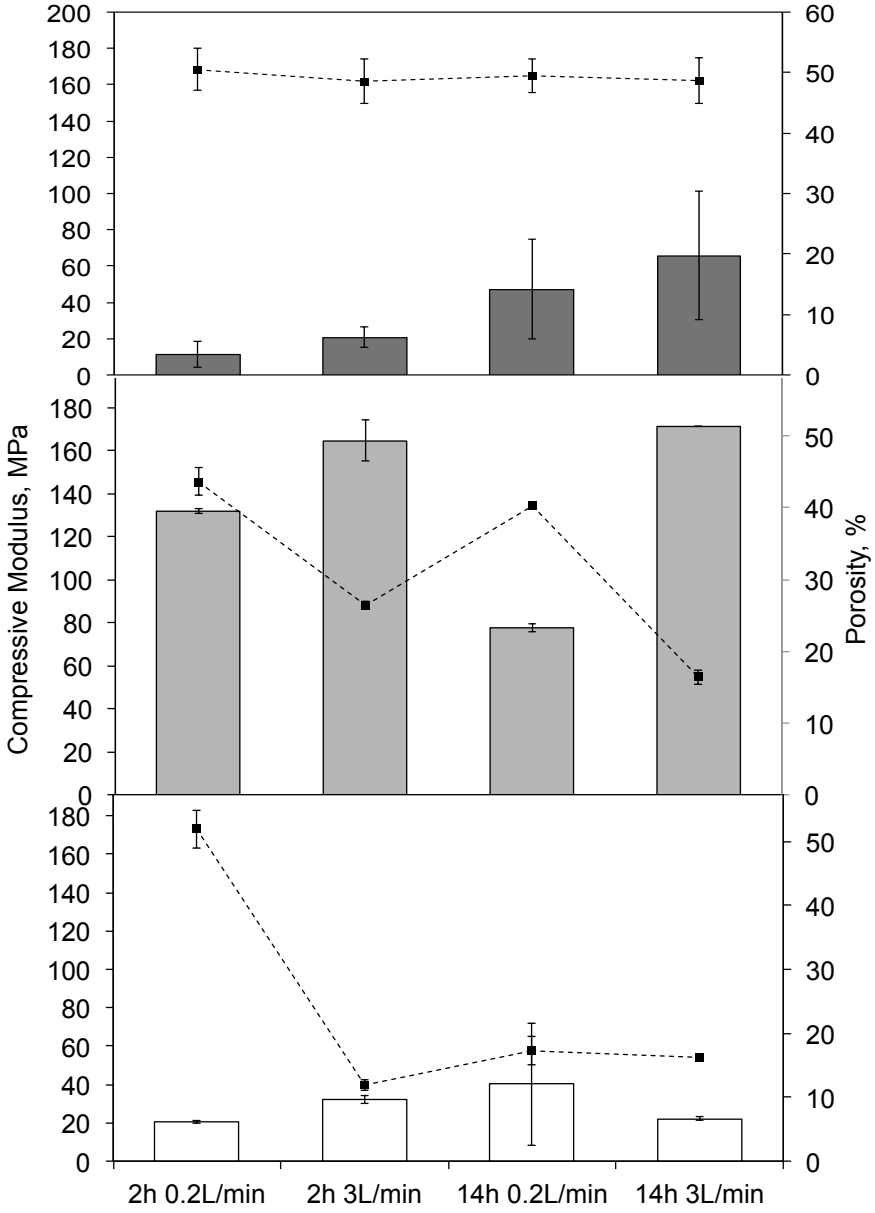

Figure 20 - Influence of porosity (−◆−) in compressive modulus of samples processed at 14 MPa 70:30,wt% (■), 90:10,wt% (■) and PCL (□).

Comparing with the neat PCL, the addition of 10% of MCM-41 SNPs caused an increase of ~30% in compressive modulus and ~15% in compressive stress, which is a general trend also observed by Mathieu *et al.* (2005), and this can be due to high porosity and pore diameter combined with thick inter-pore separation and reinforcement effect of the inorganic particles. However, in the case of higher silica amounts (30%), the constructs become brittle and lower stress and modulus are obtained; the interface separation between polymer and SNPs and higher porosity does not allow optimized contact between particles, and therefore, privileged proliferation pathways for cracks are formed, in agreement with Mathieu *et al.* (2005). The standard deviations of both properties are significant in most of the cases and can be attributed to local variations in internal porous architecture and different densities (Baker *et al.*, 2009). Nevertheless, the presence of pores present several advantages for bone re-growth over the ordinary dense materials, as explained in Section 1.1. Hence, $scCO_2$ assisted

foaming and a small amount of well-dispersed inorganic particles act like reinforcement matrix improving significantly the mechanical resistance as well as permits the development of adequate porosity for tissue growth.

A cause for some peculiar results may be due to the irregular, sometimes mushroom-like shape of the surface of the samples. Once the samples were not pretreated before analysis, the surface of the probe was likely not to compress the sample homogeneously. This means that the area of analysis (and consequently, the pressure induce by the probe on the surface) was different in some cases. One of the major drawbacks of static compression testing is that it was executed in a non-physiological environment: the hydrolytic degradation of the polymer over time enhances the decrease of mechanical properties. Nevertheless, the evaluation of these properties at time zero helps to design materials according with the intended process parameters (Baker *et al*., 2009).

3.4. Dexamethasone Sorption and Release

In order to produce drug-eluting systems, SNPs (MCM-41 and SBA-15) were loaded with DXMT by traditional liquid sorption and by supercritical solvent deposition. PCL/DXMT physical mixture was prepared by $scCO_2$-assisted foaming/mixing. DXMT-loaded SNPs were then added to PCL/2wt.%DXMT physical mixtures using also $scCO_2$-assisted foaming. Supercritical experiments were carried out at 14 MPa and 25 MPa, for 14 h and 0.2 L/min. Drug release studies were performed in order to evaluate the yields of SSD and to compare the obtained DXMT release profiles

3.4.1 Drug Sorption and Release from SNPs

Figure 21 shows MCM-41 drug-loading ability from an aqueous solution of DXMT, as a function of time. The diffusional period until drug mass becomes constant is around 5 h (7 μg/mg) and the mass variation showed in the zoomed box is owed to diffusional equilibrium. MCM-41 SNPs were efficiently DXMT-loaded from aqueous DXMT solutions corresponding to 75.8% of maximum drug sorption ability after 2.5 h and 63.9% at equilibrium (8h).

Equation (1), derived from Korsmeyer-Peppas mathematical model, was used to determine drug sorption kinetics. The *n* value represents the mechanism that rules the drug transport. Therefore, when assuming a rod-shape like geometry, when $n \leq 0.45$ the drug sorption mechanism is controlled by classic Fickian diffusion; when $n \sim 0.89$ drug release is controlled by polymer relaxation (Case transport II) and when $0.45<n<0.89$ there is a superposition between diffusion-controlled and case II-controlled transport. In this case n=0.21 which means that it is a diffusion controlled (Fickian) mechanism for drug sorption.

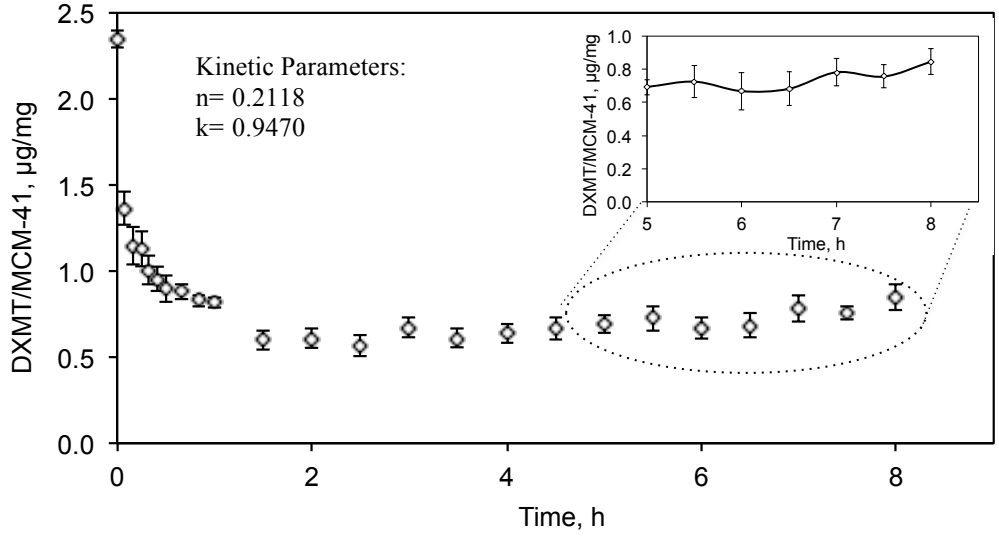

Figure 21- Drug loading ability of MCM-41 in Milli-Q water.

Also, the sorption study in ethanol was preformed and it is represented in Figure 22. It is possible to see that the sorption behavior in ethanol is very different from the sorption in water. Also, it's noticeable that there is instability along the time, but, nevertheless, the yield of sorption is considerably inferior (10.7%) to that in water and some reasons can be pointed out. Because ethanol is more volatile than water, the total volume was kept constant by adding small amounts of solvent. Also, DXMT partition coefficient between SNPs and ethanol is low in ethanol is higher than it is in inorganics/water.

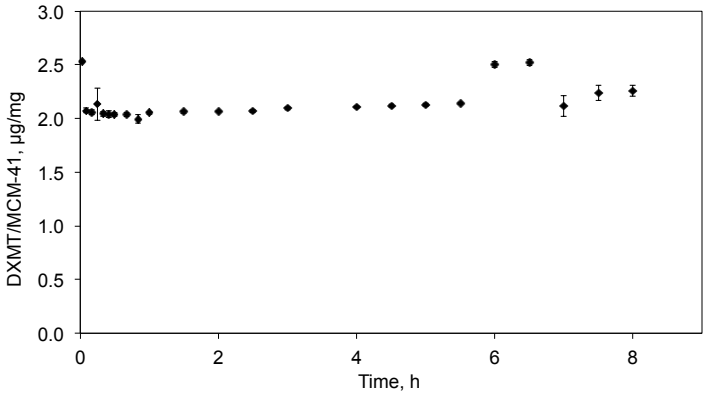

Figure 22 - Drug loading ability of MCM-41 in ethanol.

Drug aqueous sorption of SBA-15 SNPs (not shown) reveals that after 30 min the drug loading ability reaches 90.8% and once the equilibrium was reached this value decreases to 82.3 %. This sorption capability is considerably higher than in the latter case of MCM-41, which may be explained by higher pore size in SBA-15. MCM-41 supplier reports surface areas and pore sizes of 1000 m^2/g and 2.3-2.7 nm, respectively, while SBA-15 provider states 718 m^2/g and 8.5 nm correspondingly.

Regarding dexamethasone release from MCM-41 $scCO_2$ – loaded samples, as represented in Figure 23, after 8h of DXMT release in milli-Q water it was found that, for all $scCO_2$ loading conditions, the amount of DXMT released was almost constant: ~1.5 µg DXMT/mg MCM-41. After complete leaching, the total released amounts of DXMT were found to be higher than the 8h released value (Figure 27) and to vary according to the employed pressure and processing time conditions. Thus, lower pressures and longer processing times seem to increase drug deposition yields. Faster drug release rates were obtained for those samples loaded at lower pressures. This is just due to the higher amounts of loaded drug that were achieved at these specific conditions. Therefore, drug release is just controlled by diffusion, as in the case of aqueous drug sorption, since the involved specific interactions between MCM-41 and DXMT are the same for all tested conditions and no drug carrier swelling/degradation is involved in the drug release process.

Concerning drug release assays, which are represented in Figure 24, more accurate data was obtained with this material. After 8h of assay, the amount of released drug was very similar (~3µg/mg), regardless the SSD employed condition and almost two times fold than in MCM-41. The total amount, as in the previous case, was found to vary with $scCO_2$ conditions: longer SSD times and lower pressure seam to favor drug transport to the inorganic surface.

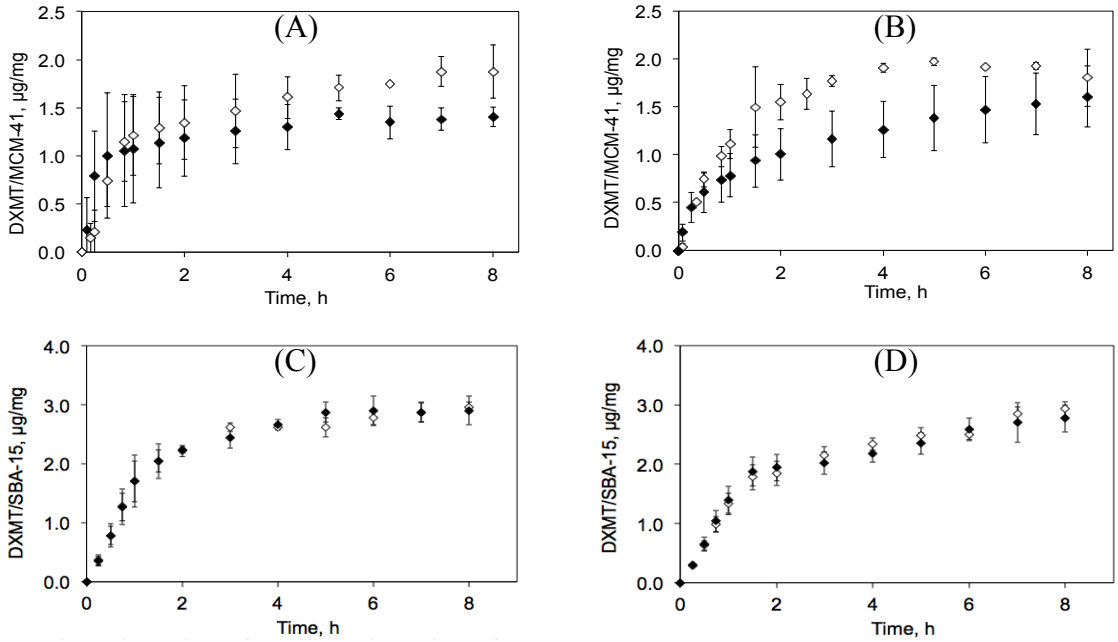

Figure 23 - MCM-41 (up row) and SBA-15 (down row) 8h drug release profile after different supercritical solvent deposition conditions: 2 h (white symbols) and 14 h (black symbols), 14 MPa (A and C) and 25 MPa (B and D)

Given that these values are so small, TGA analysis was preformed in order to verify the accuracy of the drug release results. A TGA spectrum shows thermal events of neat MCM-41 (green dashed line) and thermal behavior of drug-deposited MCM-41 (teal lines). It is evident a mass decrease that can only correspond to DXMT degradation as it can be seen in the Figure 24.

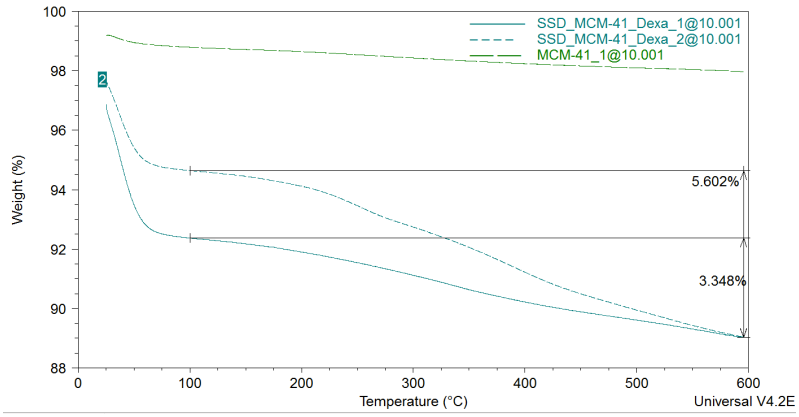

Figure 24 – Thermogravimetric analysis used to confirm the accuracy of drug released amounts from MCM-41 after SSD process.

Complete leaching was used to ease the Fickian diffusion, governed by concentration differences between SNPs and Milli-Q water, and thus determine the total amount of DXMT that could be entrapped after 72 h of release. The total amount is higher than the 8h-released amount (Figure 25). This difference can be assigned to the presence of DXMT in deeper pores, which may not allow the determination of drug in short periods of time. Also, comparing both mesoporous materials is clear that the loading ability of SBA-15 is more accurate than MCM-41, for SSD and for aqueous sorption, which in turn means that SBA-15 would be a better choice for this type of composite material. This trend can be due to the SBA-15 properties: despite the slightly lower surface area, the pores are larger, leading to an augmented and faster drug adsorption capability.

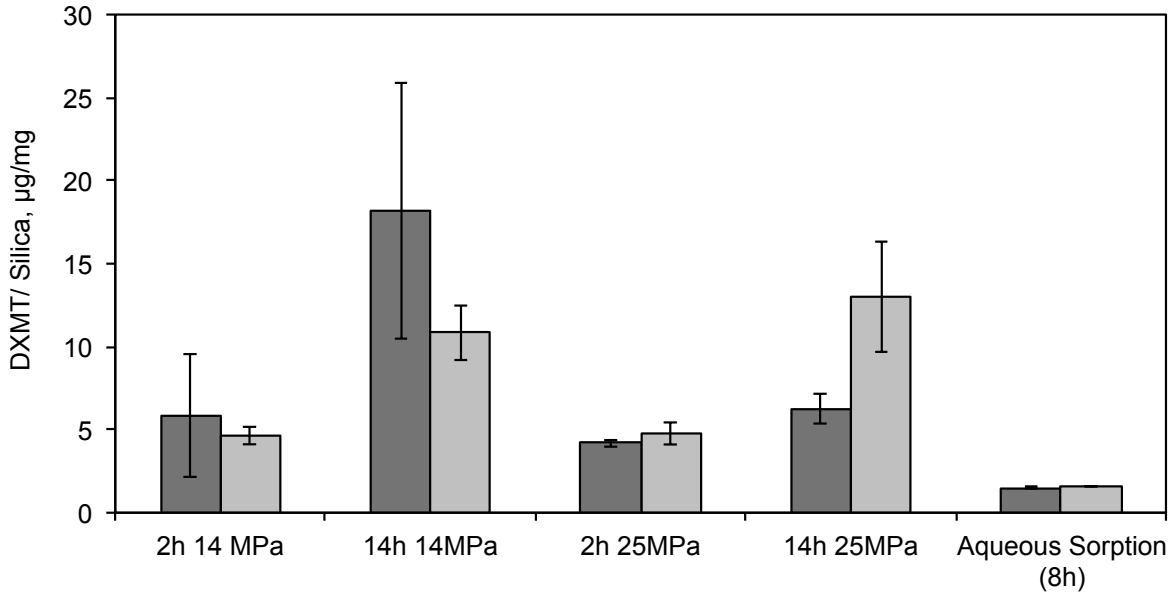

Figure 25 - Total amount of DXMT released, after leaching, and total amount of DXMT loaded by aqueous sorption from MCM-41 and SBA-15.

3.4.2 Drug Release from PCL and Composites

PCL and PCL/MCM-41 composites were also loaded with dexamethasone by physical mixture prior to $scCO_2$ processing, and the profiles are represented on Figure 26. After 7 days of drug release assay, the amount of drug released was higher for 90:10,wt.% (25 MPa) while the lower amount corresponded to PCL. Thus, considering the initial amount of DXMT, 70:30,wt.% samples released only 4.4%±0.4% (14 MPa) and 3.5%±0.4% (25 MPa), whereas 90:10,wt.% these values correspond to 4.0%±1.1% and 6.5%± 2.6% (for 14 MPa and 25 MPa, correspondingly) and PCL samples present 1.9%±0.7% (14 MPa) and 2.8%±0.1% (25 MPa). These differences may be attributed to different morphologies, different drug available sites due to different pore sizes, porosities, surface areas, and possibly different host dissolution rates when higher inorganic content is used. MCM-41 previously loaded particles were physically mixed with PCL and 2wt.% DXMT and as previously showed, these composite materials are highly heterogeneous. As previously discussed, increasing pressure and SNPs content led to higher surface areas, porosity. Thus, in drug release assays, this property will lead to significant differences. Because the drug is not only molecularly dispersed inside the polymeric/composite matrix, but also deposited on the surface, larger-pore, with higher porosity and surface areas samples will release more drug in the same period of time that in the cases where smaller-pore exist. Nevertheless, the long-term drug delivery goal can be easily accomplished using this type of materials.

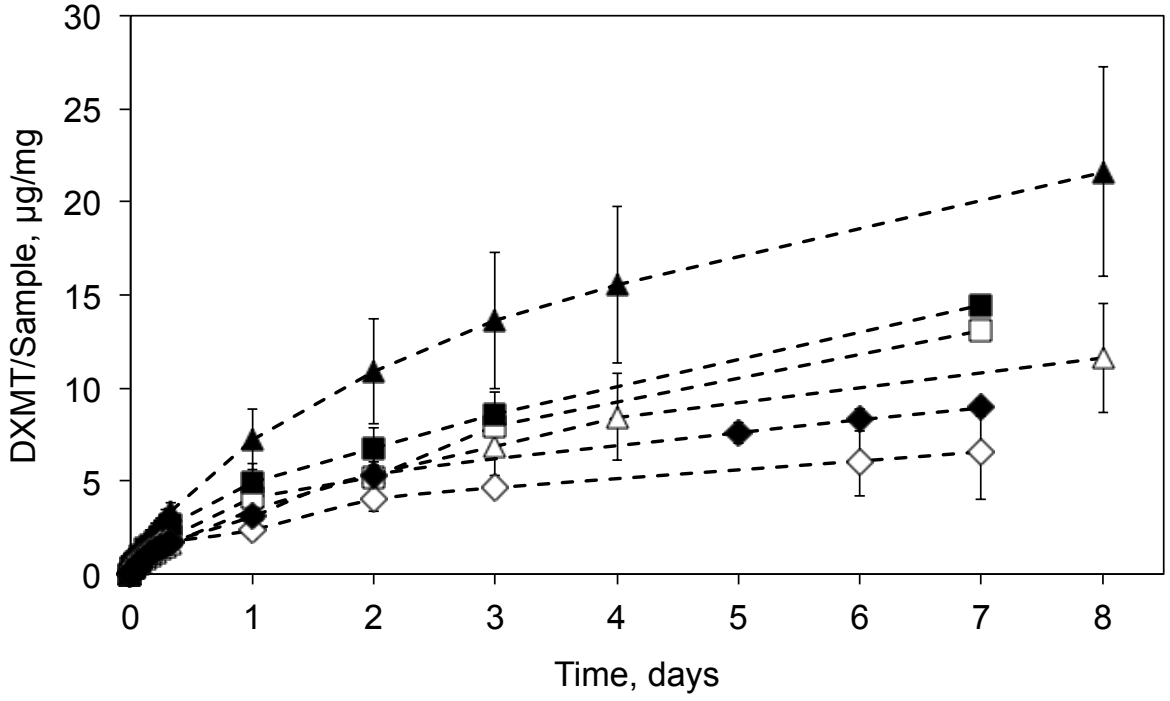

Figure 26 - DXMT release profiles from PCL (◇) PCL/MCM-41 composites 70:30,wt.% (□) and 90:10,wt.% (△) after $scCO_2$ processing at 14MPa (white symbols) and 25MPa (black symbol).

Table 5 presents the results concerning the kinetic parameters and it shows that supercritical foaming/impregnation process is tunable. In all cases, increasing pressure the release rate increases, mostly due to the higher surface areas and porosity induced by this experimental condition. For PCL samples n~0.5 and thus the release mechanism is controlled by Fick

diffusion. The remainder composites have n<0.5, which accounts for pseudo-Fickian behavior that implies that drug diffusion, and probabilly includes crystallinity and initial polymer erosion maybe occurring.

Table 3 - Kinetic parameters dexamethasone release from PCL, and 90:10,wt.% and 70:30,wt% composites processed at two different pressures, 14 h and 0.2 L/min. *l*=2mm.

Sample		Kinetic Parameters From Eq. (1), considering the first 60% of the total release			Diffusion coefficients (mm^2/day) From Equations (2) and (3)			
		k	*n*	R^2	D_1	R^2	D_2	R^2
PCL	14MPa	0.5728	0.5004	0.9504	0.1798	0.9686	0.0999	0.9978
	25MPa	0.8475	0.4744	0.9710	0.1275	0.9407	0.1353	0.9979
90:10,wt.%	14MPa	0.5784	0.2636	0.9714	0.0292	0.9446	0.0482	0.9395
	25MPa	0.6491	0.3078	0.9945	0.0425	0.9395	0.0540	0.9999
70:30,wt.%	14MPa	0.5430	0.2665	0.9833	0.0198	0.9746	0.0393	1.0000
	25MPa	0.6045	0.3196	0.9861	0.0450	0.9737	0.0720	1.0000

Considering that standard deviation errors of DXMT release from SBA-15 SNPs were smaller that from MCM-41, PCL/SBA-15 composites drug release was also studied for 14 MPa, 14h and 0.2 L/min conditions. The profiles are represented on Figure 27 and the kinetic parameters are on Table 4.

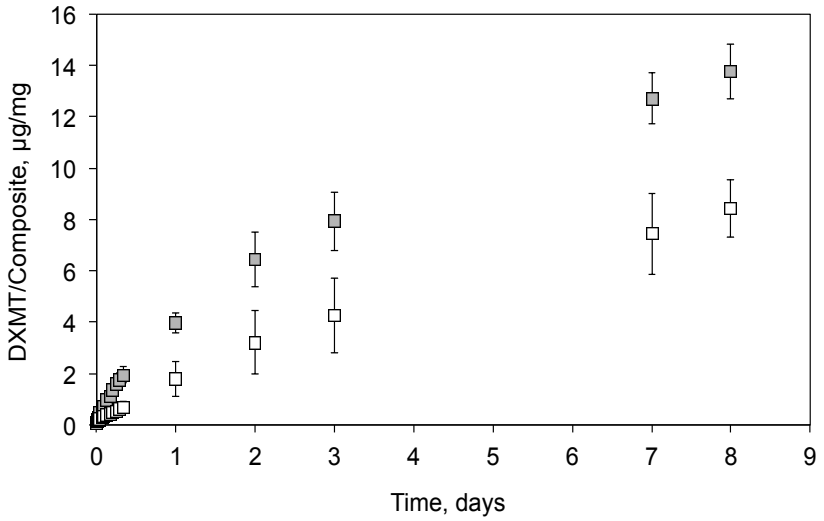

Figure 27 - DXMT release profiles from PCL/SBA-15 composites 70:30,wt.% (■) and 90:10,wt.% (□) processed at 14 MPa, 14h and 0.2 L/min.

After 8 days of drug release assay the amount of DXMT released was higher for 70:30,wt.%. Considering the initial amount of DXMT, 70:30,wt.% samples released 3.6%±0.1% whereas 90:10,wt.% present lower values of released DXMT: 2.9%±0.3%. PCL samples processed at 14 MPa presented 1.9%±0.7%, as previously seen. This was the expected tendency: higher

released amounts for 70:30,wt% and lower for PCL, while 90:10,wt% remained with an intermediate value. 70:30,wt% composites have higher porosity and surface areas, and also more quantity of drug due to higher amount of loaded-SBA-15 and also less PCL-slow degrading matrix where drug is entrapped as well. Also, in section 3.2 and although it is not the same inorganic filler, it was clear that the morphology was strongly affected by SNPs presence, which will determine the amount of drug released in a certain period a time.

Table 4 - Kinetic parameters dexamethasone release from PCL/SBA-15 composites (90:10,wt.% and 70:30,wt%) processed at 14 MPa, 14h and 0.22 L/min. *l*=2mm.

Sample	Kinetic Parameters From Eq. (1), considering the first 60% of the total release			Diffusion coefficients (mm^2/day) From Equations (2) and (3)			
	k	*n*	R^2	D_1	R^2	D_2	R^2
90:10,wt.%	0.5666	0.1713	0.9437	0.0391	0.9522	0.0331	0.9979
70:30,wt.%	0.6592	0.2833	0.9991	0.0446	0.9999	0.0683	0.9999

Because the rate of release is inferior to 0.5, pseudo-Fickian behavior is assumed and therefore that drug diffusion, crystallinity and initial polymer erosion maybe occurring and/or controlling release. Nevertheless, in the case where higher amount of SBA-15 is present, the release rate is also higher indicating that more DXMT was available near the surface, according to Fick law.

Comparing both inorganic matrices represented on Figure 28, the amount of drug released from the composite after 8 days is very similar, and the profiles are also analogous. However, the composites produced from SBA-15 reveal smaller standard errors, which may be due to more homogeneous morphology of SBA-15 composites, regarding their counterparts produced from MCM-41; however, this needs further investigation. Nevertheless, for both SNPs, the amount of released DXMT is higher for 70:30wt.% samples, which can be due to higher surface areas, higher porosity. Also, SNPs were previously loaded with the active substance and used to prepare a composite from a physical mixture of PCL/DXMT; this additionally might allow the release of slightly higher amounts of drug.

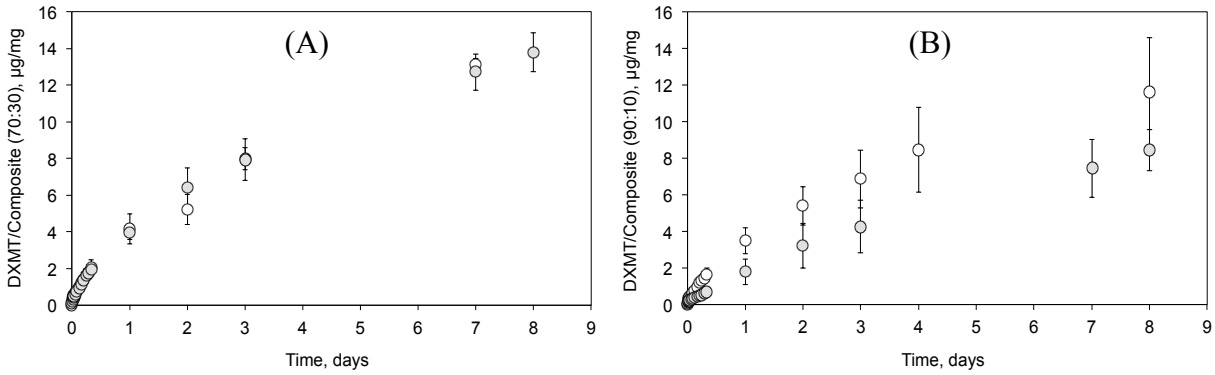

Figure 28 – Drug release comparison between composites 70:30,wt.% (A) and 90:10,wt.% (B) produced from MCM-41 (◯) and SBA-15 (◯) at 14 MPa.

Distinguishable release profiles can be obtained for several days (Figure 29), depending on the tunable supercritical conditions applied and on the host material. DXMT release from SNPs is considered as a burst release, however there are differences between MCM-41 and SBA-15. The latter is able to load higher amounts of DXMT than MCM-41, mainly due to different pore sizes. Furthermore, when these previously loaded particles are incorporated into PCL/DXMT physical mixtures, there is no longer a burst release: the polymeric matrix is able to control and sustain drug release for longer periods of time. Also, varying loaded-SNPs content in the final composite, different drug amounts are released. In the case of higher SNPs content (70:30,wt.%), there is more DXMT available next to the surface of the composite and therefore these show higher released quantities.

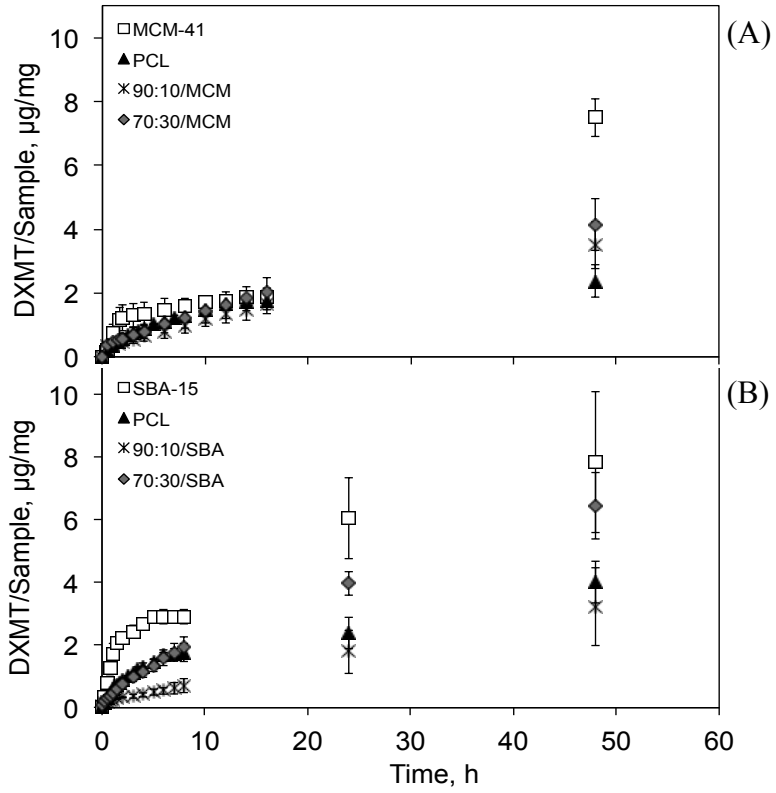

Figure 29 – Overview of dexamethasone release profiles obtained for SNPs, PCL and composites processed at 14MPa, 14 h, 0.2 L/min: MCM-41 (A) and SBA-15 (B).

It was expected that loaded polymeric and composite sample show a biphasic release behavior, with an initial period where there would be a rapid release due to DXMT deposited on/near the surface, and a slower release period on which degradation of the polymer phase would occur and the drug trapped inside would be released as this degradation occurred. The major factors that influence the first release period would be the total surface area and the porosity and pores sizes (Braga *et al.*, 2008). However, the second and slower release period was not observed because the degradation rate of PCL and materials based on this polymer are very slow, as previously stated in section 1.

For the same supercritical-assisted foaming conditions, the different amount of released drug

can be attributed to the composition of the samples and other experimental factors, like interaction of polymer/silica/drug/release medium. Samples containing 30wt.% of previously loaded SNPs are more hydrophilic and, thus, the water from the release media would reach the entrapped drug easily. By varying pressure different pore morphologies are obtained and therefore different drug release amounts are attainable. Besides this advantage, in the case of strongly hydrophobic drugs where the use of organic solvents is not inadequate, as in the case of DXMT and PCL respectively, SCF become a more appropriate solvent.

Therefore, the main purpose of this work was accomplished. Supercritical CO_2 was successfully and easily used to create drug-eluting systems based on PCL and silica nanoparticles with distinct release profiles.

Conclusions and Future Perspectives

The realization of this work presupposed the fabrication of PCL and PCL/SNPs scaffolds loaded with dexamethasone through supercritical fluids, a green technology process.

The main goals were attained: PCL/SNPs biodegradable scaffolds were produced and successfully loaded with DXMT, several working parameters where varied and studied, and distinct profiles were obtained

Thus, chemically PCL and its composites presented no chemical alteration after processing with $scCO_2$ and the presence of MCM-41 was confirmed by FTIR-ATR and SEM-EDX. Also, PCL and its PCL/MCM-41 composites showed thermic characteristic that allow them to be used in the body. The melting temperature decreases with the increase of SNPs content but it still is acceptable (above 37 ºC). Degradation temperature is also much higher than the body temperature, which makes these materials good candidates for bone tissue applications. Regarding crystallinity, this characteristic was only studied qualitatively through X-ray diffraction, and the next step would be to quantify crystallinity and compare with results easily achievable by DSC.

Pore sizes and porosities were found to be appropriate for hard tissue engineering application. To determine samples morphology, in the future is strongly recommended to use image software to determine the pore size and microCT to investigate pores interconnectivity. To further study the effect of different SNPs in the composites morphology, TEM and particle size analysis should be implemented. Nevertheless, the best morphology for tissue regrowth seams to occur in samples with 10wt.% of MCM-41 when processed at 25 MPa with low depressurization rate, and 14 MPa for 2h and low depressurization rate.

Mechanical compression tests were performed and revealed that once again 90:10,wt.% samples are more resistant because the small amount of MCM-41 had a reinforcement effect. Hereafter, compression parameters will be improved, statistical analysis will be accomplished and biomechanical mathematical models will be applied.

The use of SCF-assisted impregnation/deposition and foaming to develop drug-eluting system was also effective. In the case of SNPs, the aqueous and ethanolic sorption studies indicate that this traditional method is more time consuming and has lower yields than the supercritical deposition method. Varying the working conditions can easily change $scCO_2$-assisted drug deposition yields; in the future a suggestion is to use a co-solvent to further improve the amount of drug deposited on the inorganic material. PCL and PCL/SNPs systems in ~8days released ~4% of the initial mass of drug, with a sustained release profile, contrarily to SNPs (both MCM-41 and SBA-15) that show burst release. Unfortunately, because PCL is known for its very slow degradation, no data was collected for longer than 8days, but it would be interesting to follow this behavior for longer periods (eg. several months) and also estimate the enzymatic and hydrolytic degradation rates, pH and weight change while degradation occurs. Also, a continuous release system is being optimized and will be used to study the release kinetics more accurately and for longer periods.

Hemocompatibility assays were not performed, although there is evidence in literature that PCL is biocompatible. Concerning MCM-41 and SBA-15 compatibility is not clear and consensual among many bibliographic reviews. In this sense, PCL, mesoporous silicas, and its composites will be tested for hemocompatibility in a near future. Preliminary cell culture and in vivo tests are also proposed as a future work.

It is also suggested to study PCL/SBA-15 more profoundly, to consider different geometries of the final product (eq. screws, Figure 30), to study other molecular weight PCL, other polymers and co-polymers with restrained particle size, different molecular weights and degradation rates, and other drugs.

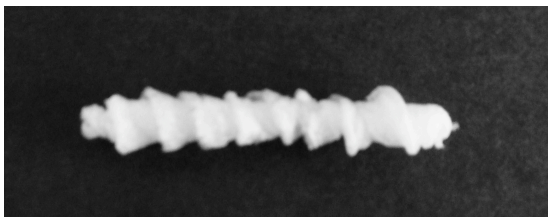

Figure 30 – Prototype of a screw produced by supercritical CO_2 foaming.

References

Anunziata O. A., Martínez M. L., Beltramone A. R., Hydroxyapatite/MCM-41 and SBA-15 Nano-Composites: Preparation, Characterization and Applications, Materials 2 (2009) 1508-1519.

Baker K. C., Bellair R., Manitiu M., Herkowitz H. N., Kannan R.M., Structure and mechanical properties of supercritical carbon dioxide processed porous resorbable polymer constructs, Journal of the Mechanical Behavior of Biomedical Materials 2 (2009) 620–626.

Belhadj-Ahmed F., Badens E., Llewellyn P., Denoyel R., Charbit G., Impregnation of vitamin E acetate on silica mesoporous phases using supercritical carbon dioxide, J. of Supercritical Fluids 51 (2009) 278–286.

Bloom S. L., Sheffield J. S., McIntire D. D., Leveno K. J., Antenatal dexamethasone and decreased birth weight, Obstetrics & Gynecology 97 (2001) 485-490.

Braga M. E. M., Pato M. V., Silva H. S. R. C., Ferreira E. I., Gil M. H., Duarte C. M. M., de Sousa H. C., Supercritical solvent impregnation of ophthalmic drugs on chitosan derivatives, Journal of Supercritical Fluids 44 (2008) 245–257.

Bronzino J. D., Park J. B., Lakes R.S., Composite Materials *in* Biomaterials – Principles and Applications, Woodhead Publishing, Cambridge, 2003.

Chrousos G. P., Detera-Wadleigh S. D., Karl M., Syndromes of glucorticoid resistance, Annals of Internal Medicine 119 (1993) 1113-1124.

Chu P. K., Chen J. Y., Wang L. P., Huang N., Plasma-surface modification of biomaterials, Materials Science and Engineering 36 (2002) 143-206.

Collins N. J., Bridson R. H., Leeke G. A., Grover L. M., Particle seeding enhances interconnectivity in polymeric scaffolds foamed using supercritical CO_2, Acta Biomaterialia 6 (2010) 1055–1060.

Collins N. J., Leeke G. A., Bridson R. H., Hassan F., Grover L. M., The influence of silica on pore diameter and distribution in PLA scaffolds produced using supercritical CO2, Journal of Materials Science: Materials in Medicine 19 (2008) 1497–1502.

Dash T. K., Konkimalla V. B., Poly-ε-caprolactone based formulations for drug delivery and tissue engineering: A review, Journal of Controlled Release (2011), doi:10.1016/j.jconrel.2011.09.064.

Dias A. M. A., Braga M. E. M., Seabra I. J., Ferreira P., Gil M. H., de Sousa H.C., Development of natural-based wound dressings impregnated with bioactive compounds and using supercritical carbon dioxide, International Journal of Pharmaceutics 408 (2011) 9–19.

Duarte A. R. C., Mano J. F., Reis R. L., Preparation of chitosan scaffolds loaded with dexamethasone for tissue engineering applications using supercritical fluid technology, European Polymer Journal 45 (2009) 141–148.

Duarte A. R. C., Mano, J. F., Reis, R. L., Dexamethasone-loaded scaffolds prepared by supercritical assisted phase inversion, Acta Biomaterialia (2009), doi: 10.1016/j.actbio.2009.01.047.

Elzubair A., Elias C. N., Suarez J. C. M., Lopes H. P., Vieira M. V. B.The physical characterization of a thermoplastic polymer for endodontic obturation, Journal of Dentistry 34 (2006) 784-789.

Fanovich M. A., Jaeger P., Sorption and diffusion of compressed carbon dioxide in polycaprolactone for the development of porous scaffolds, Materials Science and Engineering C 32 (2012) 961–968.

Georgiou G., Mathieu L., Pioletti D. P., Bourban P.-E., Månson J.-A. E., Knowles J. C., Nazhat S. N., Polylactic acid-phosphate glass composite foams as scaffolds for bone tissue engineering (2006), DOI: 10.1002/jbm.b.30600.

Harousseau J. L., Attal M., Leleu X., Troncy J., Pegourie B., Stoppa A. M., Hulin C., Benboubker L., Bortezomib plus dexamethasone as induction treatment prior to autologous stem cell transplantation in patients with newly diagnosed multiple myeloma: results of an IFM phase II study, Haematologica 91 (2006) 1498-1505.

Heikkila T., Salonen J., Tuura J., Kumar N., Salmi T., Murzin D. Y., Hamdy M. S., Mul G., Laitinen L., Kaukonen A. M., Hirvonen J., Lehto V.-P., Evaluation of Mesoporous TCPSi, MCM-41, SBA-15, and TUD-1 Materials as API Carriers for Oral Drug Delivery, Drug Delivery 14 (2007) 337–347.

Izquierdo-Barba I., Colilla M., Vallet-Regí M., Nanostructured Mesoporous Silicas for Bone Tissue Regeneration, Journal of Nanomaterials, vol. 2008, Article ID 106970, 14 pages, 2008. doi:10.1155/2008/106970.

Jenkins M. J., Harrison K. L., Silva M. M. C. G., Whitaker M. J., Shakesheff K. M., Howdle S. M., Characterisation of microcellular foams produced from semi-crystalline PCL using supercritical carbon dioxide, European Polymer Journal 42 (2006) 3145–3151.

Jenkins M., Harrison K, Introduction to polymeric scaffolds for tissue engineering *in* Biomedical Polymers, Woodhead Publishing, Cambridge, 2007.

Kikic I., Alessi P., Cortesi A., Macnaughton S.J., Foster N., Spicka B., An experimental study of supercritical adsorption equilibria of salicylic acid on activated carbon, Fluid Phase Equilibria 117 (1996) 304–311.

Kiran E., Polymer miscibility, phase separation, morphological modifications and polymorphic transformations in dense fluids, Journal of Supercritical Fluids 47 (2009) 466–483.

Lee L. J., Zeng C., Cao X., Han X., Shen J., Xu G., Polymer nanocomposite foams, Composites Science and Technology 65 (2005) 2344–2363.

Léonard A., Calberg C., Kerckhofs G., Wevers M., Jérôme R., Pirard J., Germain A., Blacher S., Characterization of the porous structure of biodegradable scaffolds obtained with supercritical CO2 as foaming agent, Journal of Porous Mater 15 (2008) 397–403.

Lin Y.-S., Haynes C. L., Impacts of Mesoporous Silica Nanoparticle Size, Pore Ordering, and Pore Integrity on Hemolytic Activity, Journal of American Chemical Society 132 (2010) 4834–4842.

Liu H., Han C., Dong L., Study on the Cell Structure and Compressive Behavior of Biodegradable Poly(e-caprolactone) Foam, Polymer Engineering and Science (2008), doi: 10.1002/pen.21199.

Liu X., Poon R. W. Y., Kwok S. C. H., Chu P.K., Ding C., Plasma surface modification of titanium for hard tissue replacements, Surface & Coatings Technology 18 (2004) 227-233.

Long J. D., Xu S., Cai J. W., Jiang N., Lu J. H., Ostrikov K. N., Diong C. H., Structure, bonding state and in vitro study of Ca-P-Ti film deposited on Ti6A14V by RF magnetron sputtering, Materials Science and Engineering 20 (2002) 175-180.

López-Periago A., Argemí A., Andanson J. M., Fernández V., García-González C. A., Kazarian S. G., Saurina J., Domingo C., Impregnation of a biocompatible polymer aided by supercritical CO2: Evaluation of drug stability and drug–matrix interactions, Journal of Supercritical Fluids 48 (2009) 56–63.

Lui S. Q., Biomaterial Aspects of Bioregenerative Engineering *in* Bioregenerative Engineering – Principles and Applications, John Wiley & Sons, New Jersey, 2007.

Mathieu L. M., Montjovent M.-O., Bourban P-E., Pioletti D. P., Månson J.-A. E., Bioresorbable composites prepared by supercritical fluid foaming (2005), DOI: 10.1002/jbm.a.30385.

Meyer U., Meyer T., Handschel J., Wiesmann H. P., Djouad F., Tuan R. S., Mesenchymal Stem Cells: New Insights Into Tissue Engineering and Regenerative Medicine *in* Fundamentals of Tissue Engineering and Regenerative Medicine, Springer, Berlin, 2009.

Morèrea J., Tenorioa M. J., Torralvob M. J., Pandoa C., Renuncioa J. A. R., Cabañas A., Deposition of Pd into mesoporous silica SBA-15 using supercritical carbon dioxide, Journal of Supercritical Fluids 56 (2011) 213–222.

Natu M. V., Gaspar M. N., Ribeiro C. A. F., Cabrita A. M., de Sousa H. C., Gil M. H., In vitro and in vivo evaluation of an intraocular implant for glaucoma treatment, International Journal of Pharmaceutics 415 (2011) 73–82.

Natu M. V., Gil M. H., de Sousa H. C., Supercritical solvent impregnation of poly(ε-caprolactone)/ poly (oxyethylene-b-oxypropylene-b-oxyethylene) and poly(ε-caprolactone)/ poly(ethylene-vinyl acetate) blends for controlled release applications, J. of Supercritical Fluids 47 (2008) 93–102.

Paital S. R., Dahortre N. B., Calcium Phosphate coatings for bio-implant applications: Materials, performance factors, and methodologies, Materials Science and Engineering 66 (2009) 1-70.

Park J., Lakes R. S., Introduction *in* Biomaterials – An Introduction, Springer, 3rd Edition, New York, 2007.

Pitt C. G., Chasin M., Langer R., Poly-ε-caprolactone and its copolymers *in* Biodegradable Polymers as Drug Delivery Systems, Marcel Dekker, New York, 1990.

Provan D., Stasi R., Newland A. C., *et al.*, International consensus report on the investigation and management of primary immune thrombocytopenia, Blood Journal 115 (2010) 168-186.

Ratner B. D., Migliaresi C., Alexander H., Composites *in* Biomaterials Science, Elsevier Academic Press, 2004.

Roohani-Esfahani S. I., Nouri-Khorasani S., Lu Z. F., Appleyard R. C., Zreiqat H., Effects of bioactive glass nanoparticles on the mechanical and biological behavior of composite coated scaffolds, Acta Biomaterialia 7 (2011) 1307–1318.

Schemelzeisen R., Frölich J. C., Prevention of postoperative swelling and pain by dexamethasone after operative removal of impacted third molar teeth, European Journal of clinical Pharmacology 44 (2004) 275-277.

Shieh Y.-T., Lai J.-G., Tang W.-L., Yang C.-H., Wang T.-L., Supercritical CO_2 intercalation of polycaprolactone in layered silicates, Journal of Supercritical Fluids 49 (2009) 385–393.

Smirnova I., Suttiruengwong S., Arlt W., Feasibility study of hydrophilic and hydrophobic silica aerogels as drug delivery systems, Journal of Non-Crystalline Solids 350 (2004) 54–60.

Smith W. F., Materiais Poliméricos *in* Princípios de ciência e engenharia dos materiais, McGraw-Hill, Lisboa, 1998.

Tai H., Popov V.K., Shakesheff K. M., Howdle S. M., Putting the fizz into chemistry: applications of supercritical carbon dioxide in tissue engineering, drug delivery and synthesis of novel block copolymers, Biochemical Society Transactions 35 (2007) 516-521.

Takahashi M., Ushijima K., Hayashi Y., Maekawa T., Ando H., Tsuruoka S.-ichi, Fujimura A., Dosing-time dependent effect of dexamethasone on bone density in rats, Life Sciences 86 (2010) 24–29.

Tsimpliaraki A., Tsivintzelis I., Marras S.I., Zuburtikudis I., Panayiotou C., The effect of surface chemistry and nanoclay loading on the microcellular structure of porous poly(d,l lactic acid) nanocomposites, Journal of Supercritical Fluids 57 (2011) 278–287.

Vallet-Regí M., Balas F., Arcos D., Mesoporous materials for drug delivery, Angewandte. Chemie International Edition 46 (2007) 7548 – 7558.

Vallet-Regí M., Colilla M., González B, Medical applications of organic-inorganic hybrid materials within the field of silica-based bioceramics, Chemical Society Reviews 40 (2011) 596-607.

van de Beek D., de Gans J., McIntyre P., Prasad K. B., Corticosteroids for acute bacterial meningitis, Cochrane Database of Systematic Reviews 2010, Issue 9, Art. No.: CD004405. doi: 10.1002/14651858.CD004405.pub3.

Vega-González A., Subra-Paternault P., López-Periago A. M., García-González C. A., Domingo C., Supercritical CO_2 antisolvent precipitation of polymer networks of L-PLA, PMMA and PMMA/PCL blends for biomedical applications, European Polymer Journal 44

(2008) 1081–1094.

Woods H. M., Silva M. M. C. G., Nouvel C., Shakesheffb K. M., Howdle S. M., Materials processing in supercritical carbon dioxide: surfactants, polymers and biomaterials, Journal of Materials Chemistry 14 (2004) 1663–1678.

Xu Q., Ren X., Chang Y., Wang J., Yu L., Dean K., Generation of microcellular biodegradable polycaprolactone foams in supercritical carbon dioxide, Journal of Applied Polymer Science 94 (2004) 593–597.

Yañez F., Martikainen L., Braga M. E. M., A.-Lorenzo C., Concheiro A., Duarte C. M. M., Gil M. H., de Sousa H. C. Supercritical fluid-assisted preparation of imprinted contact lenses for drug delivery, Acta Biomaterialia 7 (2011) 1019–1030.

Yoon J. J., Kim J. H., Park T. G., Dexamethasone-releasing biodegradable polymer scaffolds fabricated by a gas-foaming/ salt- leaching method, Biomaterials 24 (2003) 2323-2329.

Yu T., Malugin A., Ghandehari H., Impact of silica nanoparticle design on cellular toxicity and hemolytic activity, Journal of American Chemical Society 7 (2011) 5717–5728.

Zhai W., Yu J., Wu L., Ma W., He J., Heterogeneous nucleation uniformizing cell size distribution in microcellular nanocomposites foams, Polymer 47 (2006) 7580-7589.

Zhao Y., Sun X., Zhang G., Trewyn B. G., Slowing I. I., Lin V. S.-Y., Interaction of mesoporous silica nanoparticles with human red blood cell membranes: size and surface effects, Journal of American Chemical Society 2 (2011) 1366–1375.

Supplementary Data

Appendix A

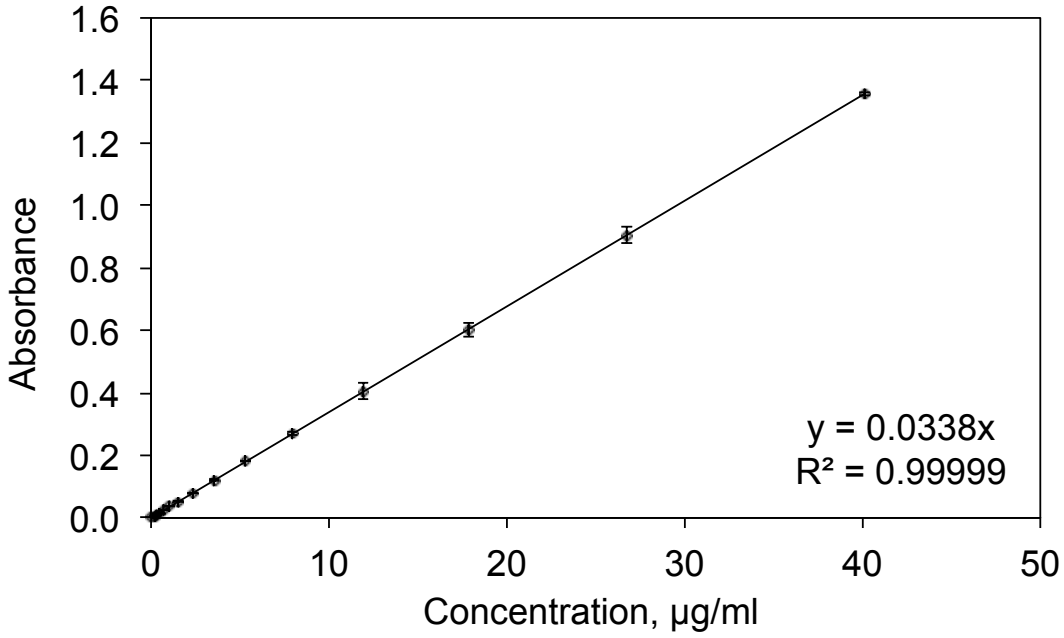

Figure A1 – Dexamethasone standard curve in Milli-Q water, used to determine the amount of drug in spectrophotometric experiments (wavelength = 242 nm).

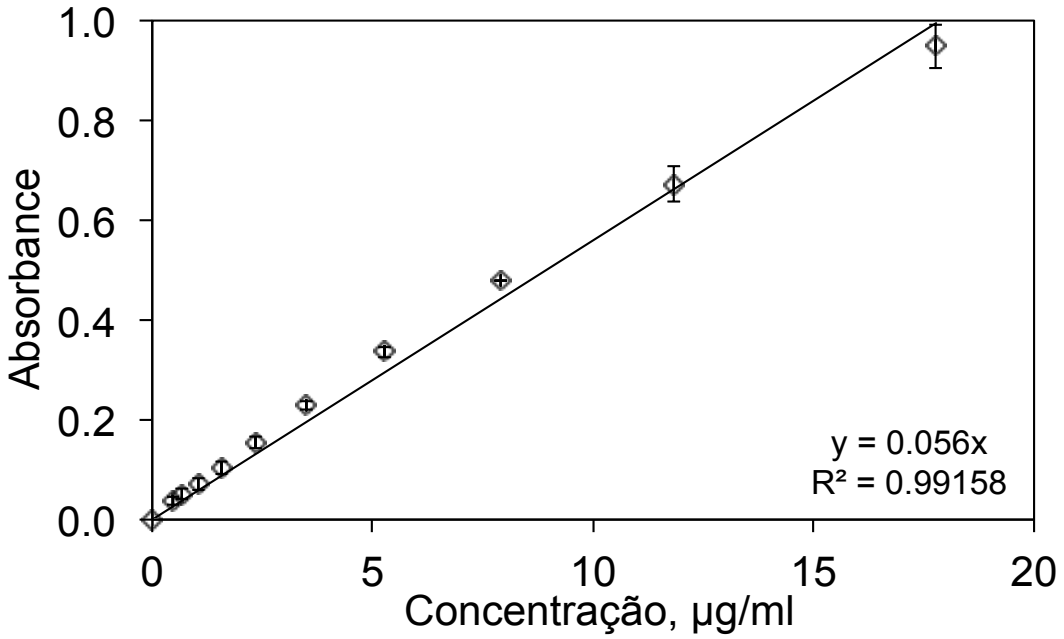

Figure A2 – Dexamethasone standard curve in ethanol, used to determine the amount of drug in spectrophotometric experiments (wavelength = 242 nm).

Appendix B

Table B1 - Results obtained from Nitrogen Adsorption for all samples processed by $scCO_2$: Surface Area, Pore Volume and Average Pore Diameter.

Sample		Surface Area, m^2/g			Pore Volume, cm^3/g			Average Pore Diameter, Å		
		Average	Standard Deviation	Variation Coefficient %	Average	Standard Deviation	Variation Coefficient %	Average	Standard Deviation	Variation Coefficient %
70:30,wt.% 14 MPa	2h 0.2 L/min	20.5393	0.6689	3.2564	0.0399	0.0021	5.3699	77.6258	1.6416	2.1148
	2h 3.0 L/min	16.5575	2.9626	17.8930	0.0286	0.0102	35.4798	53.5906	0.3737	0.6973
	14h 0.2 L/min	13.3575	1.8183	13.6128	0.0272	0.0122	44.6773	111.7561	22.1781	19.8451
	14h 3.0 L/min	11.1803	1.5597	13.9502	0.0146	0.0004	2.57889	52.8037	6.0146	11.3905
90:10,wt.% 14 MPa	2h 0.2 L/min	1.9549	0.0557	2.8503	0.0046	0.0018	38.6600	130.1296	16.5568	12.7234
	2h 3.0 L/min	1.7375	0.4407	25.3670	0.0055	0.0024	44.2870	76.2354	10.0409	13.1709
	14h 0.2 L/min	1.9058	0.2843	14.9154	0.0052	0.0023	43.7936	140.7438	0.6683	0.4748
	14h 3.0 L/min	1.2730	0.1093	8.5875	0.0024	0.0006	24.3847	79.2638	28.3888	35.8156
PCL 14 MPa	2h 0.2 L/min	0.9152	0.2281	24.9249	0.0016	0.0003	17.7345	68.5976	5.0681	7.3882
	2h 3.0 L/min	0.6213	0.0339	5.4629	0.0014	0.0005	33.6568	72.9646	12.3477	16.9229
	14h 0.2 L/min	0.8279	0.0388	4.6805	0.0018	0.0002	10.3341	85.9651	13.9139	16.1856
	14h 3.0 L/min	0.65110	0.05006	7.68901	0.00158	0.00002	1.3839	96.5795	6.0785	6.2938
70:30,wt.% 25 MPa	2h 0.2 L/min	17.5023	5.9957	34.2566	0.0296	0.0041	13.8829	65.0738	26.4363	40.6251
	2h 3.0 L/min	68.8399	27.7758	40.3485	0.0856	0.0322	37.6682	50.01615	1.4508	2.9006
	14h 0.2 L/min	75.2438	9.3130	12.3771	0.0922	0.0208	22.5787	42.7570	0.6802	1.5909
	14h 3.0 L/min	134.6965	5.5771	4.1405	0.1511	0.0515	34.0706	41.3319	3.8894	9.4103
90:10,wt.% 25 MPa	2h 0.2 L/min	2.2112	0.3912	17.6905	0.0070	0.0008	11.1477	130.5423	37.2761	28.5548
	2h 3.0 L/min	1.3285	0.6009	45.2384	0.0023	0.0007	29.2951	70.9819	12.1281	17.0862
	14h 0.2 L/min	15.1885	0.5693	3.7482	0.0297	0.0079	26.7030	60.5016	1.8289	3.02295
	14h 3.0 L/min	39.5896	16.2254	40.9840	0.0444	0.0146	32.8706	45.6839	3.9749	8.7008
PCL 25 MPa	2h 0.2 L/min	0.7774	0.0781	10.0418	0.0016	0.0001	2.9548	80.3220	5.6858	7.0788
	2h 3.0 L/min	0.5191	0.0434	8.3638	0.0009	0.0002	25.3387	68.3383	11.7445	17.1858
	14h 0.2 L/min	0.6489	0.0574	8.8484	0.0014	0.0001	4.8319	87.6419	3.5385	4.0375
	14h 3.0 L/min	0.6497	0.0761	11.7107	0.0009	0.0004	46.8235	59.0347	9.9274	16.8163

Table B2 - Results obtained from Mercury Intrusion for all samples processed by $scCO_2$: Average Pore Diameter and Porosity.

Sample		Average Pore Diameter, μm			Porosity, %		
		Average	Standard deviation	Variation Coefficient, %	Average	Standard Deviation	Variation Coefficient, %
70:30,wt.% 14 MPa	2h 0.2 L/min	0.7254	0.2812	38.7573	50.5296	3.4669	6.8612
	2h 3.0 L/min	0.2080	0.0321	15.4340	48.5704	3.6828	7.5825
	14h 0.2 L/min	6.8049	1.2361	18.1649	49.4933	2.7930	5.6432
	14h 3.0 L/min	0.3162	0.0012	0.3802	48.69595	3.7938	7.7909
90:10,wt.% 14 MPa	2h 0.2 L/min	0.2539	0.0520	20.4975	43.6573	1.9011	4.3545
	2h 3.0 L/min	0.1403	0.0395	28.1834	26.4022	0.6395	2.4222
	14h 0.2 L/min	0.2249	0.0220	9.7803	40.1971	0.2029	0.5047
	14h 3.0 L/min	0.1079	0.0170	15.8009	16.3466	0.9615	5.8821
PCL 14 MPa	2h 0.2 L/min	0.1093	0.0175	15.9868	51.9025	2.9298	5.6449
	2h 3.0 L/min	0.0684	0.0148	21.7094	11.8802	0.8461	7.1221
	14h 0.2 L/min	0.4029	0.0829	20.5892	17.2606	2.1881	12.6767
	14h 3.0 L/min	0.0857	0.0013	1.4852	16.1208	0.3637	2.2563
70:30,wt.% 25 MPa	2h 0.2 L/min	0.3151	0.0387	12.2770	55.3655	0.3276	0.5917
	2h 3.0 L/min	39.4498	8.3161	21.0802	46.1659	1.5922	3.4488
	14h 0.2 L/min	1.5019	0.2524	16.8037	47.5828	2.3236	4.8833
	14h 3.0 L/min	0.2204	0.0822	37.3209	55.2296	0.0531	0.0962
90:10,wt.% 25 MPa	2h 0.2 L/min	0.2550	0.0399	15.6395	43.6214	1.5886	3.6418
	2h 3.0 L/min	0.1534	0.0160	10.4176	21.9852	0.6235	2.8361
	14h 0.2 L/min	0.2609	0.0327	12.5509	50.3729	5.9013	11.7152
	14h 3.0 L/min	0.1161	0.0051	4.3852	27.5439	1.5493	5.6250
PCL 25 MPa	2h 0.2 L/min	0.2442	0.0199	8.1656	45.4203	1.3678	3.0113
	2h 3.0 L/min	0.0933	0.0127	13.6419	11.9234	1.6484	13.8250
	14h 0.2 L/min	0.0922	0.0052	5.6016	22.0875	0.9955	4.5069
	14h 3.0 L/min	0.0800	0.0035	4.4194	16.3578	0.9005	5.5050

Table B3 – Comparison between density results obtained from Helium Picnometry and from Mercury Intrusion for all samples processed by $scCO_2$.

Sample		Helium Picnometry			Mercury Intrusion					
		Density, g/cm^3			Aparent Density, g/ml			Bulk Density, g/ml		
		Average	Standard Deviation	Variation Coefficient, %	Average	Standard Deviation	Variation Coefficient, %	Average	Standard Deviation	Variation Coefficient, %
70:30,wt.% 14 MPa	2h 0.2 L/min	1.2608	0.0092	0.7324	1.0521	0.1044	9.9201	0.5187	0.0151	2.9173
	2h 3.0 L/min	1.2368	0.0036	0.2906	1.201	0.025	2.097	0.618	0.057	9.247
	14h 0.2 L/min	1.2688	0.0102	0.8032	1.2006	0.0252	2.0967	0.6179	0.0571	9.2465
	14h 3.0 L/min	1.2568	0.0226	1.7960	1.1256	0.1539	13.6766	0.5664	0.0463	8.1779
90:10,wt.% 14 MPa	2h 0.2 L/min	1.1461	0.0033	0.2843	1.2310	0.0042	0.3389	0.6316	0.0488	7.7249
	2h 3.0 L/min	1.1511	0.0125	1.0831	1.1337	0.0174	1.5343	0.6389	0.0314	4.9140
	14h 0.2 L/min	1.1320	0.0154	1.3561	1.1588	0.0216	1.8672	0.8977	0.0866	9.6497
	14h 3.0 L/min	1.1502	0.0050	0.4371	1.1328	0.0020	0.1748	0.6775	0.0035	0.5115
PCL 14 MPa	2h 0.2 L/min	1.0896	0.0104	0.9528	1.1796	0.0177	1.4986	0.9867	0.0034	0.3440
	2h 3.0 L/min	1.1260	0.0015	0.1334	1.1307	0.0040	0.3502	0.7607	0.2754	36.2083
	14h 0.2 L/min	1.1106	0.0127	1.1448	1.1386	0.0047	0.4161	1.0033	0.0054	0.5356
	14h 3.0 L/min	1.1144	0.0073	0.6536	1.1268	0.0167	1.4810	0.7068	0.2737	38.7295
70:30,wt.% 25 MPa	2h 0.2 L/min	1.2685	0.0073	0.5734	1.1517	0.0073	0.6324	0.9660	0.0103	1.0687
	2h 3.0 L/min	1.3088	0.0162	1.2351	1.2357	0.0018	0.1431	0.5515	0.0048	0.8719
	14h 0.2 L/min	1.3107	0.0098	0.7470	0.9009	0.0617	6.8525	0.4845	0.0189	3.8972
	14h 3.0 L/min	1.2902	0.0069	0.5383	0.9767	0.1012	10.3606	0.5108	0.0303	5.9393
90:10,wt.% 25 MPa	2h 0.2 L/min	1.1437	0.0068	0.5921	1.2167	0.0037	0.3022	0.5448	0.0023	0.4284
	2h 3.0 L/min	1.1564	0.0048	0.4176	1.1605	0.0044	0.3778	0.6543	0.0209	3.1989
	14h 0.2 L/min	1.1721	0.0193	1.6466	1.1602	0.0063	0.5425	0.9040	0.0137	1.5175
	14h 3.0 L/min	1.1734	0.0060	0.5100	1.1300	0.0440	3.8922	0.5621	0.0885	15.7498
PCL 25 MPa	2h 0.2 L/min	1.0996	0.0146	1.3312	1.1490	0.0187	1.6247	0.8327	0.0313	3.7621
	2h 3.0 L/min	1.1283	0.0148	1.3127	1.1071	0.0175	1.5840	0.6044	0.0247	4.0834
	14h 0.2 L/min	1.0954	0.0145	1.3273	1.1419	0.0108	0.9475	1.0058	0.0283	2.8121
	14h 3.0 L/min	1.1083	0.0049	0.4429	1.1375	0.0006	0.0559	0.8862	0.0109	1.2288

Appendix C

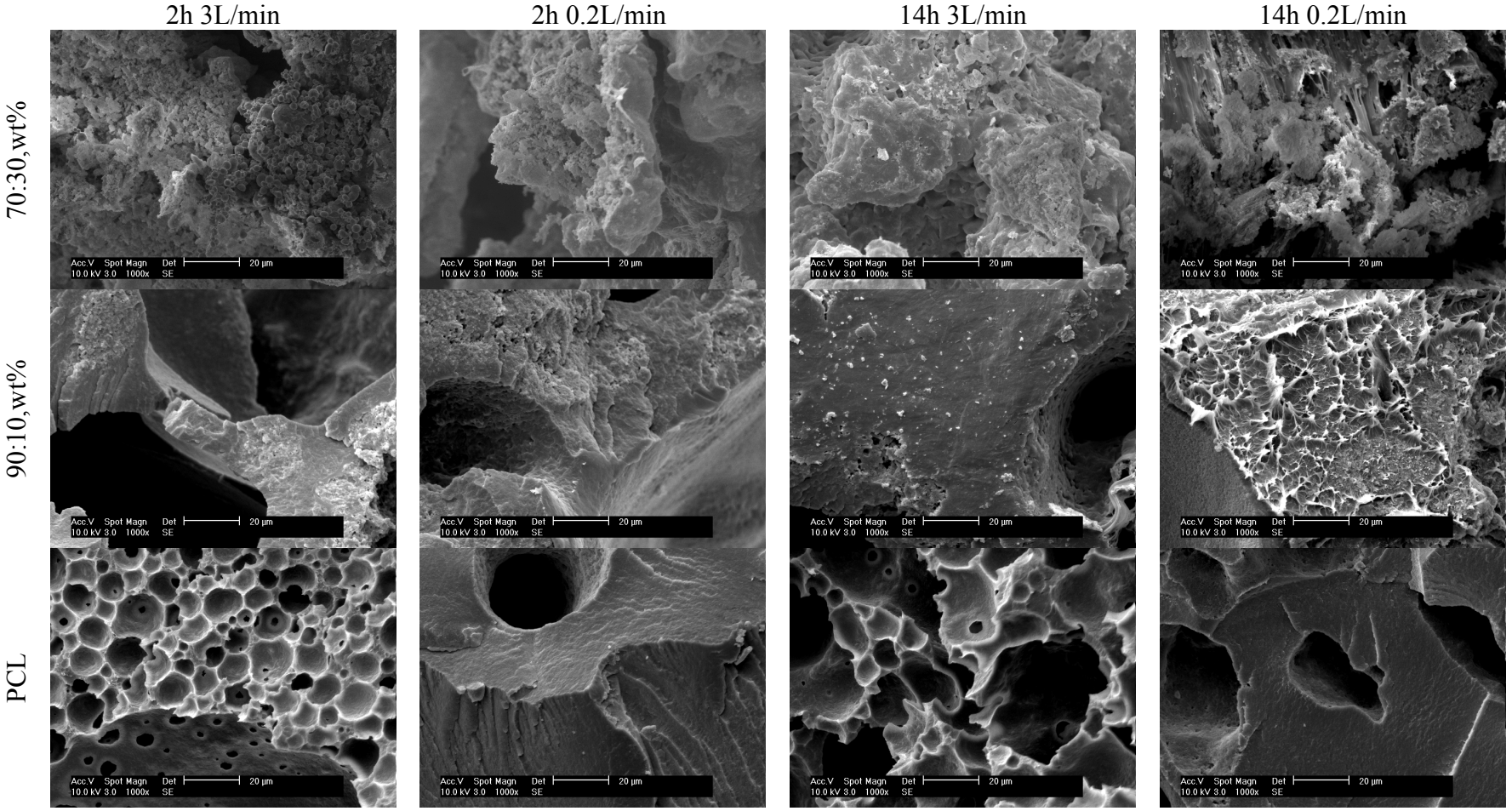

Figure C1 - SEM of samples processed at 14 MPa. Magnification 1000x. Scale bar 20 µm.

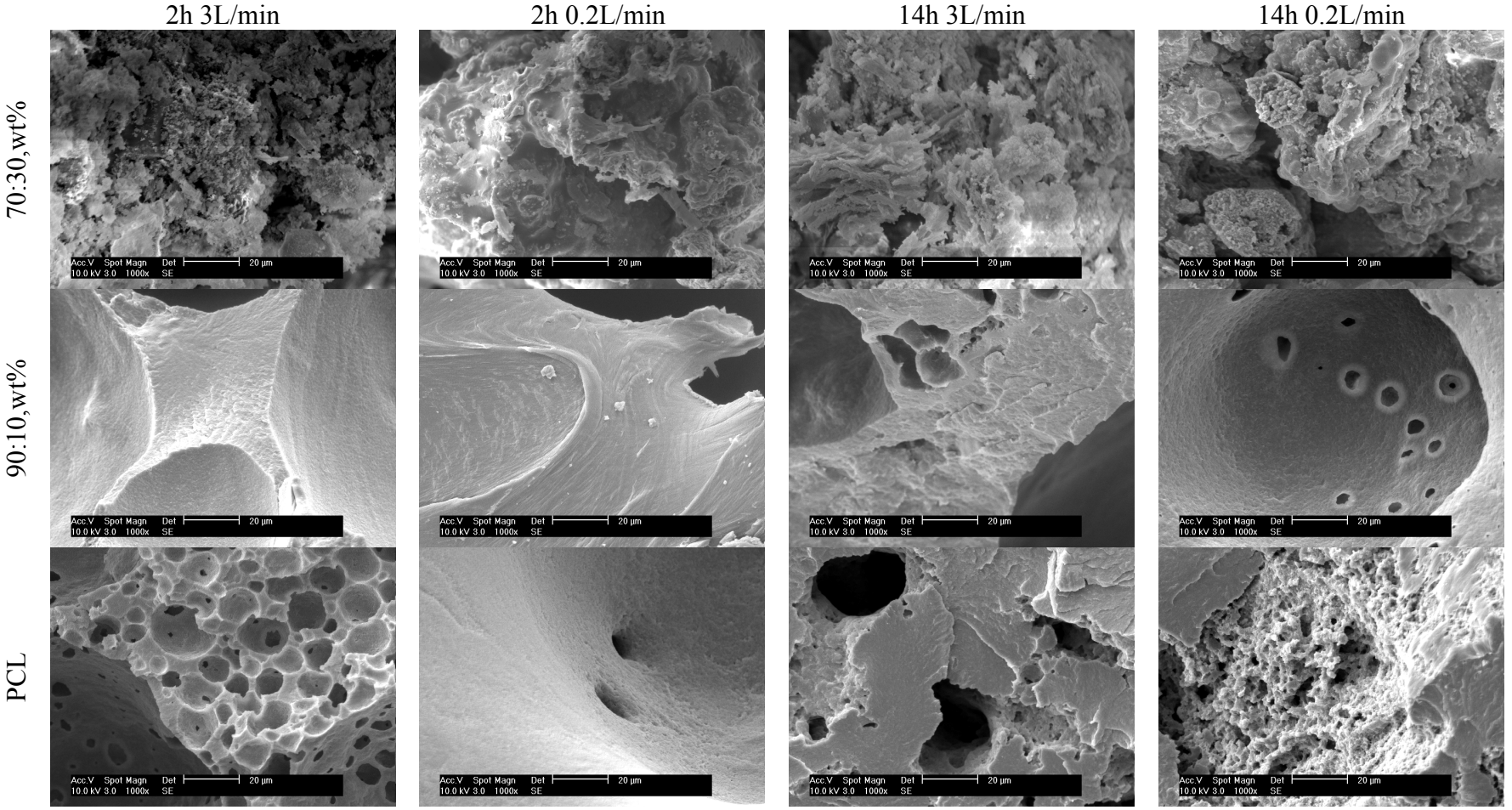

Figure C2 - SEM of samples processed at 25 MPa. Magnification 1000x. Scale bar 20 μm.